

EQUATIONS AND ALGORITHMS FOR MIXED-FRAME FLUX-LIMITED DIFFUSION RADIATION HYDRODYNAMICS

MARK R. KRUMHOLZ¹

Department of Astrophysical Sciences, Princeton University, Princeton, NJ 08544; krumholz@astro.princeton.edu

RICHARD I. KLEIN

Department of Astronomy, University of California, Berkeley, CA 94720; and Lawrence Livermore National Laboratory,
 P.O. Box 808, L-23, Livermore, CA 94550; klein@astron.berkeley.edu

CHRISTOPHER F. MCKEE

Departments of Physics and Astronomy, University of California, Berkeley, CA 94720; cmckee@astron.berkeley.edu

AND

JOHN BOLSTAD

Lawrence Livermore National Laboratory, P.O. Box 808, L-23, Livermore, CA 94550; bolstad@llnl.gov

Received 2006 October 16; accepted 2007 May 24

ABSTRACT

We analyze the mixed-frame equations of radiation hydrodynamics under the approximations of flux-limited diffusion and a thermal radiation field and derive the minimal set of evolution equations that includes all terms that are of leading order in any regime of nonrelativistic radiation hydrodynamics. Our equations are accurate to first order in v/c in the static diffusion regime. In contrast, we show that previous lower order derivations of these equations omit leading terms in at least some regimes. In comparison to comoving-frame formulations of radiation hydrodynamics, our equations have the advantage that they manifestly conserve total energy, making them very well suited to numerical simulations, particularly with adaptive meshes. For systems in the static diffusion regime, our analysis also suggests an algorithm that is both simpler and faster than earlier comoving-frame methods. We implement this algorithm in the Orion adaptive mesh refinement code and show that it performs well in a range of test problems.

Subject headings: hydrodynamics — methods: numerical — radiative transfer

1. INTRODUCTION

Astrophysical systems described by radiation hydrodynamics span a tremendous range of scales and parameter regimes, from the interiors of stars (e.g., Kippenhahn & Weigert 1994) to accretion disks around compact objects (e.g., Turner et al. 2003) to dusty accretion flows around massive protostars (e.g., Krumholz et al. 2005, 2007) to galactic-scale flows onto active galactic nuclei (e.g., Thompson et al. 2005). All of these systems have in common that matter and radiation are strongly interacting and that the energy and momentum carried by the radiation field are significant in comparison to those carried by the gas. Thus, an accurate treatment of the problem must include analysis both of the matter and the radiation and of their interaction.

Numerical methods exist to simulate such systems in a variety of dimensionalities and levels of approximation. In three dimensions, treatments of the matter and radiation fields generally adopt the flux-limited diffusion approximation, first introduced by Alme & Wilson (1973) for reasons of computational cost and simplicity (e.g., Hayes et al. 2006). Flux-limited diffusion is optimal for treating continuum transfer in a system such as an accretion disk, stellar atmosphere, or opaque interstellar gas cloud where the majority of the interesting behavior occurs in optically thick regions that are well described by pure radiation diffusion, but there is a surface of optical depth unity from which energy is radiated away. Applying pure diffusion to these problems would lead to unphysically fast radiation from this surface, so flux-limited diffusion provides a compromise that yields a computationally simple

and accurate description of the interior, while also giving a reasonably accurate loss rate from the surface (Castor 2004).

However, the level of accuracy provided by this approximation has been unclear, because the equations of radiation hydrodynamics for flux-limited diffusion have previously only been analyzed to zeroth order in v/c . In contrast, several authors have analyzed the radiation hydrodynamic equations in the general case to beyond first order in v/c (e.g., Mihalas & Weibel-Mihalas 1999; Castor 2004 and references therein). In a zeroth-order treatment, one neglects differences between quantities in the laboratory frame and the comoving frame. The problem with this approach is that in an optically thick fluid the radiation flux only follows Fick's law ($\mathbf{F} \propto -\nabla E$) in the comoving frame, and in other frames, there is an added advective flux of radiation enthalpy, as first demonstrated by Castor (1972). In certain regimes (i.e., the dynamic diffusion limit—see below), this advective flux can dominate the diffusive flux (Mihalas & Auer 2001; Castor 2004).

Pomraning (1983) does give a flux-limiter usable to first order in v/c , which is an approach to the problem of flux-limiting with relativistic corrections that is an alternative to the one we pursue in this paper. However, this approach does not correctly handle the dynamic diffusion limit, a case that, as we show, requires special attention, because order v^2/c^2 terms can be important. Furthermore, Pomraning derives his flux-limiter directly from the transfer equation, so the computation provides little insight into the relative importance of radiation hydrodynamic terms, and the level of accuracy obtained by using the uncorrected flux-limiter, the most common procedure in astrophysical applications.

Mihalas & Klein (1982) were the first to derive the mixed-frame equations of radiation hydrodynamics dynamics to order

¹ Hubble Fellow.

v/c in frequency-integrated and frequency-dependent forms and gave numerical algorithms for solving them. Lowrie et al. (1999), Lowrie & Morel (2001), and Hubeny & Burrows (2007) give alternate forms of these equations, as well as numerical algorithms for solving them. However, these treatments require that one solve the radiation momentum equation (and for the frequency-dependent equations calculate over many frequencies as well), rather than adopt the flux-limited diffusion approximation. While this is preferable from a standpoint of accuracy, since it allows explicit conservation of both momentum and energy and captures the angular dependence of the radiation field in a way that diffusion methods cannot, treating the radiation momentum equation is significantly more computationally costly than using flux-limited diffusion, making it difficult to use in three-dimensional calculations.

In this paper we analyze the equations of radiation hydrodynamics under the approximations that the radiation field has a thermal spectrum and obeys the flux-limited diffusion approximation and that scattering is negligible for the system. Our goal is to derive an accurate set of mixed-frame equations, meaning that radiation quantities are written in the lab frame, but fluid quantities, in particular fluid opacities, are evaluated in the frame comoving with the fluid. This formulation is optimal for three-dimensional simulations, because writing radiation quantities in the lab frame lets us use an Eulerian grid on which the radiative transfer problem can be solved by any number of standard methods, while avoiding the need to model the direction- and velocity-dependence of the lab frame opacity and emissivity of a moving fluid.

In § 2 we begin from the general lab frame equations of hydrodynamics to first order in v/c , apply the flux-limited diffusion approximation in the frame comoving with the gas where it is applicable, and transform the appropriate radiation quantities into the lab frame, thereby deriving the corresponding mixed-frame equations suitable for implementation in numerical simulations. We retain enough terms to ensure that we achieve order unity accuracy in all regimes and order v/c accuracy for static diffusion problems. In § 3 we assess the significance of the higher order terms that appear in our equations and consider where treatments omitting them are acceptable and where they are likely to fail. We show that, in at least some regimes, the zeroth-order treatments most often used are likely to produce results that are incorrect at order unity. We also compare our equations to the comoving-frame equations commonly used in other codes. In § 4 we take advantage of the ordering of terms we derive for the static diffusion regime to construct a radiation hydrodynamic simulation algorithm for static diffusion problems that is simpler and faster than those now in use, which we implement in the Orion adaptive mesh refinement code. In § 5 we demonstrate it in a selection of test problems. Finally, we summarize our results in § 6.

2. DERIVATION OF THE EQUATIONS

In the discussion that follows, we adopt the convention of writing quantities measured in the frame comoving with a fluid with a subscript zero. Quantities in the lab frame are written without subscripts. We write scalars in italics (e.g., a), vectors in bold italic (e.g., \mathbf{a}), and rank 2 tensors in boldface (e.g., \mathbf{A}). We indicate tensor contractions over a single index by dots (e.g., $\mathbf{a} \cdot \mathbf{b} = a^i b_i$), tensor contractions over two indices by colons (e.g., $\mathbf{A} : \mathbf{B} = A^{ij} B_{ij}$), and tensor products of vectors without any operator symbol [e.g., $(\mathbf{ab})^{ij} = a^i b^j$]. In addition, note that we follow the standard convention in radiation hydrodynamics rather than the standard in astrophysics, in that when we refer to an opacity κ we

mean the total opacity, measured in units of inverse length, rather than the specific opacity, measured in units of length squared divided by mass. Since we are neglecting scattering, we can set the extinction $\chi = \kappa$.

2.1. Regimes of Radiation Hydrodynamics

Before beginning our analysis, it is helpful to examine some characteristic dimensionless numbers for a radiation hydrodynamic system, since evaluating these quantities provides a useful guide to how we should analyze our equations. Let ℓ be the characteristic size of the system under consideration, u be the characteristic velocity in this system, and $\lambda_p \sim 1/\kappa$ be the photon mean free path. Following Mihalas & Weibel-Mihalas (1999) we can define three distinct limiting cases by considering the dimensionless ratios $\tau \equiv \ell/\lambda_p$, which characterizes the optical depth of the system, and $\beta \equiv u/c$, which characterizes how relativistic it is. Since we focus on nonrelativistic systems, we assume $\beta \ll 1$. We term the case $\tau \ll 1$, in which the radiation and gas are weakly coupled, the “streaming” limit. If $\tau \gg 1$, then radiation and gas are strongly coupled, and the system is in the diffusion limit. We can further subdivide the diffusion limit into the cases $\beta \gg \tau^{-1}$ and $\beta \ll \tau^{-1}$. The former is the “dynamic diffusion” limit, while the latter is the “static diffusion” limit. In summary, the limiting cases are

$$\tau \ll 1, \quad (\text{streaming limit}), \quad (1)$$

$$\tau \gg 1, \quad \beta\tau \ll 1, \quad (\text{static diffusion limit}), \quad (2)$$

$$\tau \gg 1, \quad \beta\tau \gg 1, \quad (\text{dynamic diffusion limit}). \quad (3)$$

Physically, the distinction between static and dynamic diffusion is that, in dynamic diffusion, radiation is principally transported by advection by gas, so that terms describing the work done by radiation on gas and the advection of radiation enthalpy dominate over terms describing either diffusion or emission and absorption. In the static diffusion limit the opposite holds. A paradigmatic example of a dynamic diffusion system is a stellar interior. The optical depth from the core to the surface of the Sun is $\tau \sim 10^{11}$, and typical convective and rotational velocities are $\gg 10^{-11}c = 0.3 \text{ cm s}^{-1}$, so the Sun is strongly in the dynamic diffusion regime. In contrast, an example of a system in the static diffusion limit is a relatively cool, dusty, outer accretion disk around a forming massive protostar, as studied, e.g., by Krumholz et al. (2007). The specific opacity of gas with the standard interstellar dust abundance to infrared photons is $\kappa/\rho \sim 1 \text{ cm}^2 \text{ g}^{-1}$, and at distances of more than a few AU from the central star, the density is generally $\rho \lesssim 10^{-12} \text{ g cm}^{-3}$. For a disk of scale height $h \sim 10 \text{ AU}$, the optical depth to escape is

$$\tau^{-1} \approx 6.7 \times 10^{-3} \left(\frac{\kappa/\rho}{\text{cm}^2 \text{ g}^{-1}} \right)^{-1} \times \left(\frac{\rho}{10^{-12} \text{ g cm}^{-3}} \right)^{-1} \left(\frac{h}{10 \text{ AU}} \right)^{-1}. \quad (4)$$

The velocity is roughly the Keplerian speed, so

$$\beta \approx 1.4 \times 10^{-4} \left(\frac{M_*}{10 M_\odot} \right)^{1/2} \left(\frac{r}{10 \text{ AU}} \right)^{-1/2}, \quad (5)$$

where M_* is the mass of the star and r is the distance from it. Thus, this system is in a static diffusion regime by roughly 2 orders of magnitude.

In the analysis that follows, our goal is to obtain expressions that are accurate for the leading terms in all regimes. This is somewhat tricky, particularly for diffusion problems, because we are attempting to expand our equations simultaneously in the two small parameters β and $1/\tau$. The most common approach in radiation hydrodynamics is to expand expressions in powers of β alone and to only analyze the equations in terms of τ after dropping terms of high order in β . However, this approach can produce significant errors, because terms in the radiation hydrodynamic equations proportional to the opacity are multiplied by a quantity of order τ . Thus, in our derivation we repeatedly encounter expressions proportional to $\beta^2\tau$, and in a problem that is either in the dynamic diffusion limit or close to it ($\beta\tau \gtrsim 1$), it is inconsistent to drop these terms while retaining ones that are of order β . We therefore retain all terms up to order β^2 in our derivation, unless we explicitly check that they are not multiplied by terms of order τ and can therefore be dropped safely.

2.2. The Equations of Radiation Hydrodynamics

We now start our derivation, beginning from the lab frame equations of radiation hydrodynamics (Mihalas & Klein 1982; Mihalas & Weibel-Mihalas 1999; Mihalas & Auer 2001)

$$\frac{\partial \rho}{\partial t} + \nabla \cdot (\rho \mathbf{v}) = 0, \quad (6)$$

$$\frac{\partial}{\partial t}(\rho \mathbf{v}) + \nabla \cdot (\rho \mathbf{v} \mathbf{v}) = -\nabla P + \mathbf{G}, \quad (7)$$

$$\frac{\partial}{\partial t}(\rho e) + \nabla \cdot [(\rho e + P)\mathbf{v}] = cG^0, \quad (8)$$

$$\frac{\partial E}{\partial t} + \nabla \cdot \mathbf{F} = -cG^0, \quad (9)$$

$$\frac{1}{c^2} \frac{\partial \mathbf{F}}{\partial t} + \nabla \cdot \mathbf{P} = -\mathbf{G}, \quad (10)$$

where ρ , \mathbf{v} , e , and P are the density, velocity, specific energy (thermal plus kinetic), and thermal pressure of the gas, respectively, E , \mathbf{F} , and \mathbf{P} are, respectively, the radiation energy density, flux, and pressure tensor,

$$cE = \int_0^\infty d\nu \int d\Omega I(\mathbf{n}, \nu), \quad (11)$$

$$\mathbf{F} = \int_0^\infty d\nu \int d\Omega \mathbf{n} I(\mathbf{n}, \nu), \quad (12)$$

$$c\mathbf{P} = \int_0^\infty d\nu \int d\Omega \mathbf{n} \mathbf{n} I(\mathbf{n}, \nu), \quad (13)$$

(G^0 , \mathbf{G}) is the radiation four-force density

$$cG^0 = \int_0^\infty d\nu \int d\Omega [\kappa(\mathbf{n}, \nu) I(\mathbf{n}, \nu) - \eta(\mathbf{n}, \nu)], \quad (14)$$

$$c\mathbf{G} = \int_0^\infty d\nu \int d\Omega [\kappa(\mathbf{n}, \nu) I(\mathbf{n}, \nu) - \eta(\mathbf{n}, \nu)] \mathbf{n}, \quad (15)$$

and $I(\mathbf{n}, \nu)$ is the intensity of the radiation field at frequency ν traveling in direction \mathbf{n} . Here $\kappa(\mathbf{n}, \nu)$ and $\eta(\mathbf{n}, \nu)$ are the direction- and frequency-dependent radiation absorption and emission coefficients in the lab frame. Intuitively, we can understand cG^0 as the rate of energy absorption from the radiation field minus the rate of energy emission for the fluid and \mathbf{G} as the rate of momentum absorption from the radiation field minus the rate of momentum emission. Equations (6)–(8) are accurate to first order

in v/c , while equations (9)–(10) are exact. Note that no terms involving opacity or optical depth appear explicitly in any of these equations, so the fact that they are accurate to first order in β means that they include all the leading-order terms.

Mihalas & Auer (2001) show that, if the flux spectrum of the radiation is direction-independent, the radiation four-force on a thermally emitting material to all orders in v/c is given in terms of moments of the radiation field by

$$\begin{aligned} G^0 &= \gamma [\gamma^2 \kappa_{0E} + (1 - \gamma^2) \kappa_{0F}] E - \gamma \kappa_{0P} a_R T_0^4 \\ &\quad - \gamma (\mathbf{v} \cdot \mathbf{F} / c^2) [\kappa_{0F} - 2\gamma^2 (\kappa_{0F} - \kappa_{0E})] \\ &\quad - \gamma^3 (\kappa_{0F} - \kappa_{0E}) (\mathbf{v} \mathbf{v}) : \mathbf{P} / c^2, \end{aligned} \quad (16)$$

$$\begin{aligned} \mathbf{G} &= \gamma \kappa_{0F} (\mathbf{F} / c) - \gamma \kappa_{0P} a_R T_0^4 (\mathbf{v} / c) \\ &\quad - [\gamma^3 (\kappa_{0F} - \kappa_{0E}) (\mathbf{v} / c) E + \gamma \kappa_{0F} (\mathbf{v} / c) \cdot \mathbf{P}] \\ &\quad + \gamma^3 (\kappa_{0F} - \kappa_{0E}) [2\mathbf{v} \cdot \mathbf{F} / c^3 - (\mathbf{v} \mathbf{v}) : \mathbf{P} / c^3] \mathbf{v}, \end{aligned} \quad (17)$$

where $\gamma = 1/(1 - v^2/c^2)^{1/2}$ is the Lorentz factor and T_0 is the gas temperature. The three opacities that appear are the Planck, energy, and flux mean opacities, which are defined by

$$\kappa_{0P} = \frac{\int_0^\infty d\nu \kappa_0(\nu) B(\nu, T_0)}{B(T_0)}, \quad (18)$$

$$\kappa_{0E} = \frac{\int_0^\infty d\nu \kappa_0(\nu) E_0(\nu)}{E_0}, \quad (19)$$

$$\kappa_{0F} = \frac{\int_0^\infty d\nu \kappa_0(\nu) \mathbf{F}_0(\nu)}{\mathbf{F}_0}, \quad (20)$$

respectively, where $E_0(\nu)$ and $\mathbf{F}_0(\nu)$ are the comoving-frame radiation energy and flux per unit frequency, E_0 and \mathbf{F}_0 are the corresponding frequency-integrated energy and flux, and $B(\nu, T) = (2h\nu^3/c^2)/(e^{h\nu/k_B T} - 1)$ and $B(T) = ca_R T^4/(4\pi)$ are the frequency-dependent and frequency-integrated Planck functions.

Note that we have implicitly assumed that the opacity and emissivity are directionally independent in the fluid rest frame, which is the case for any conventional material. We have also assumed that the flux spectrum is independent of direction, allowing us to replace the flux mean opacity vector with a scalar. This may not be the case for an optically thin system, or one in which line transport is important, but since we are limiting our application to systems to which we can reasonably apply the diffusion approximation, this is not a major limitation.

To simplify (G^0 , \mathbf{G}), first we assume that the radiation has a blackbody spectrum, so that $E_0(\nu) \propto B(\nu, T_0)$. In this case, clearly

$$\kappa_{0E} = \kappa_{0P}. \quad (21)$$

Second, we adopt the flux-limited diffusion approximation (see below), so in optically thick parts of the flow $\mathbf{F}_0(\nu) \propto -\nabla E_0(\nu)/\kappa_0(\nu)$ (Fick's law). This implies that $\mathbf{F}_0(\nu) \propto -[\partial B(\nu, T_0)/\partial T_0](\nabla T_0)/\kappa_0(\nu)$, and substituting this into equation (20) shows that the flux mean opacity κ_{0F} is equal to the Rosseland mean opacity, defined by

$$\kappa_{0R}^{-1} = \frac{\int_0^\infty d\nu \kappa_0(\nu)^{-1} [\partial B(\nu, T_0)/\partial T_0]}{\int_0^\infty d\nu [\partial B(\nu, T_0)/\partial T_0]}. \quad (22)$$

TABLE 1
SCALINGS OF TERMS IN THE RADIATION FOUR-FORCE DENSITY

Term	G^0 or \mathbf{G}	Streaming	Static Diffusion	Dynamic Diffusion
$\kappa_{0P}(E - 4\pi B/c) \dots\dots\dots$	G^0	τ^*	$1/\tau^*$	$\beta^2 \tau^*$
$(\kappa_{0R} - 2\kappa_{0P})(\mathbf{v} \cdot \mathbf{F}/c^2) \dots\dots\dots$	G^0	$\beta\tau$	β	$\beta^2 \tau^*$
$(v/c)^2(\kappa_{0P} - \kappa_{0R})E \dots\dots\dots$	G^0	$\beta^2 \tau$	$\beta^2 \tau$	$\beta^2 \tau^*$
$(1/2)(v/c)^2 \kappa_{0P}(4\pi B/c - E) \dots\dots\dots$	G^0	$\beta^2 \tau$	β^2/τ	$\beta^4 \tau$
$(\kappa_{0R} - \kappa_{0P})(\mathbf{v}\mathbf{v}/c^2) : \mathbf{P} \dots\dots\dots$	G^0	$\beta^2 \tau$	$\beta^2 \tau$	$\beta^2 \tau^*$
$\kappa_{0R} \mathbf{F}/c \dots\dots\dots$	\mathbf{G}	τ^*	1^*	$\beta\tau^*$
$\kappa_{0P}(\mathbf{v}/c)(4\pi B/c - E) \dots\dots\dots$	\mathbf{G}	$\beta\tau$	β/τ	$\beta^3 \tau$
$\kappa_{0R}[(\mathbf{v}/c)E + (\mathbf{v}/c) \cdot \mathbf{P}] \dots\dots\dots$	\mathbf{G}	$\beta\tau$	$\beta\tau$	$\beta\tau^*$
$(1/2)(v/c)^2 \kappa_{0R} \mathbf{F}/c \dots\dots\dots$	\mathbf{G}	$\beta^2 \tau$	β^2	$\beta^3 \tau$
$2(\kappa_{0R} - \kappa_{0P})(\mathbf{v} \cdot \mathbf{F})\mathbf{v}/c^3 \dots\dots\dots$	\mathbf{G}	$\beta^2 \tau$	β^2	$\beta^3 \tau$

NOTES.—Col. (2): Whether the term appears in G^0 or \mathbf{G} . Col. (3)–(5): All scalings are normalized to E/ℓ . The scalings that are of leading order in each regime are denoted by an asterisk.

In optically thin parts of the flow, $|\mathbf{F}_0(\nu_0)| \rightarrow cE_0(\nu_0)$, so in principle we should have $\kappa_{0F} = \kappa_{0E}$. However, interpolating between these cases is complex, and the flux-limited diffusion approximation is of limited accuracy for optically thin flows in complex geometries. Moreover, our approximation that the radiation spectrum is that of a blackbody at the local radiation temperature is itself problematic in the optically thin limit, so setting $\kappa_{0F} = \kappa_{0P}$ would not necessarily be more accurate than using κ_{0R} . We therefore choose to optimize our accuracy in the optically thick part of the flow and set

$$\kappa_{0F} = \kappa_{0R}. \quad (23)$$

With these two approximations, the only two opacities remaining in our equations are κ_{0R} and κ_{0P} , both of which are independent of the spectrum of the radiation field and the direction of radiation propagation and which can therefore be tabulated as a function of temperature for a given material once and for all.

Next, we expand (G^0, \mathbf{G}) in powers of v/c , retaining terms to order v^2/c^2 . In performing this expansion, we note that $|\mathbf{F}| \leq cE$, and $\text{Tr}(\mathbf{P}) = E$. The resulting expression for the radiation four-force is

$$\begin{aligned} G^0 &= \kappa_{0P} \left(E - \frac{4\pi B}{c} \right) + (\kappa_{0R} - 2\kappa_{0P}) \frac{\mathbf{v} \cdot \mathbf{F}}{c^2} \\ &+ \frac{1}{2} \left(\frac{v}{c} \right)^2 \left[2(\kappa_{0P} - \kappa_{0R})E + \kappa_{0P} \left(E - \frac{4\pi B}{c} \right) \right] \\ &+ (\kappa_{0P} - \kappa_{0R}) \frac{\mathbf{v}\mathbf{v}}{c^2} : \mathbf{P} + O\left(\frac{v^3}{c^3}\right), \end{aligned} \quad (24)$$

$$\begin{aligned} \mathbf{G} &= \kappa_{0R} \frac{\mathbf{F}}{c} + \kappa_{0P} \left(\frac{\mathbf{v}}{c} \right) \left(E - \frac{4\pi B}{c} \right) - \kappa_{0R} \left(\frac{\mathbf{v}}{c} E + \frac{\mathbf{v}}{c} \cdot \mathbf{P} \right) \\ &+ \frac{1}{2} \left(\frac{v}{c} \right)^2 \kappa_{0R} \frac{\mathbf{F}}{c} + 2(\kappa_{0R} - \kappa_{0P}) \frac{(\mathbf{v} \cdot \mathbf{F})\mathbf{v}}{c^3} + O\left(\frac{v^3}{c^3}\right). \end{aligned} \quad (25)$$

It is helpful at this point, before we making any further approximations, to examine the scalings of these terms with the help of our dimensionless parameters β and τ . In the streaming limit, radiation travels freely at c , and emission and absorption of radiation by matter need not balance, so $|\mathbf{F}| \sim cE$ and $4\pi B/c - E \sim E$. For static diffusion, Mihalas & Weibel-Mihalas (1999) show that $|\mathbf{F}| \sim cE/\tau$ and $4\pi B/c - E \sim E/\tau^2$. For dynamic diffusion, radiation travels primarily by advection, so

$|\mathbf{F}| \sim vE$. We show in the Appendix that for dynamic diffusion $4\pi B/c - E \sim \beta^2 E$. Note that the scaling $4\pi B/c - E \sim (\beta/\tau)E$ given in Mihalas & Weibel-Mihalas (1999) appears to be incorrect, as we show in the Appendix. Using these values, we obtain the scalings shown in Table 1 for the terms in equations (24) and (25).

Table 1 shows that, despite the fact that we have kept all terms that are formally order β^2 or more, in fact we only have leading-order accuracy in the dynamic diffusion limit, because in this limit, the order unity and order β terms in G^0 vanish to order β^2 . To obtain the next-order terms, we would have had to write G^0 to order β^3 . A corollary of this is that treatments of the dynamic diffusion limit that do not retain order β^2 terms are likely to produce equations that are incorrect at order unity, since they will have dropped terms that are of the same order as the ones that have been retained.

At this point we could begin dropping terms that are insignificant at the order to which we are working, but it is cumbersome to construct a table analogous to Table 1 at every step of our derivation. It is more convenient to continue our analysis retaining all the terms in equations (24) and (25) and to drop terms only periodically.

Before moving on, there is a subtlety in equations (24) and (25) that is worth commenting on. Consider a gray fluid, one in which $\kappa_{0R} = \kappa_{0P} = \kappa_0$. In cG^0 , the term that describes the work done by radiation, $-\kappa_0 \mathbf{v} \cdot \mathbf{F}/c$, has the opposite sign from what one might naively expect. Using cG^0 in the gas energy equation (8) in this case implies that the gas energy increases when \mathbf{v} and \mathbf{F} are antialigned, i.e., when gas moves into an oncoming photon flux. We can understand the origin of this somewhat counter-intuitive behavior by considering the example of a fluid in thermal equilibrium with a radiation field in its rest frame (i.e., $4\pi B = cE_0$). In the comoving frame, the radiation four-force behaves as one intuitively expects. At leading order, the rate at which the radiation field transfers momentum density to the gas is $\mathbf{G}_0 = \kappa_0 \mathbf{F}_0/c$, and the rate at which the gas energy density changes as a result is $cG_0^0 = \kappa_0 \mathbf{v} \cdot \mathbf{F}_0/c$ (Mihalas & Auer 2001, their eqs. [53a] and [53b]). Thus, gas loses energy when it moves opposite the direction of the flux and, hence, opposite the force.

However, now consider the fluid as seen by an observer in a frame boosted by velocity $-\mathbf{v}$ relative to the fluid. The observer sees the radiation energy density as E , which differs from E_0 by $2\mathbf{v} \cdot \mathbf{F}/c^2$ (see eq. [31]), and this difference is the reason that the work term in G^0 is $-\kappa_0 \mathbf{v} \cdot \mathbf{F}/c^2$. Physically, this happens because an observer who sees the fluid moving at velocity \mathbf{v} also sees the radiation and gas as being out of thermal equilibrium ($4\pi B \neq cE$),

since E and E_0 are different. This disequilibrium leads the radiation and gas to exchange energy at a rate that is opposite in direction and twice as large as the radiation work, $\kappa_0 \mathbf{v} \cdot \mathbf{F}/c$. This is why the “work” term has the opposite sign than the one we might expect. Thus, for the rest of this paper, while for convenience we continue to refer to $(\kappa_{0R} - 2\kappa_{0P})\mathbf{v} \cdot \mathbf{F}/c$ and the terms to which it gives rise as “work” terms, it is important to keep in mind that in reality this term contains contributions from two different effects of comparable magnitude, the “Newtonian work” $\kappa_{0R}\mathbf{v} \cdot \mathbf{F}/c$ and the post-Newtonian term $-2\kappa_{0P}\mathbf{v} \cdot \mathbf{F}/c$ describing the imbalance between emission and absorption that an observer sees solely because the fluid is moving.

With this point understood, we now adopt the flux-limited diffusion approximation (Alme & Wilson 1973), under which we drop radiation momentum equation (10) and set the radiation flux in the comoving frame to

$$\mathbf{F}_0 = -\frac{c\lambda}{\kappa_{0R}} \nabla E_0, \quad (26)$$

where λ is a dimensionless number called the flux-limiter. Many functional forms for λ are possible. For the code implementation we describe below, we adopt the Levermore & Pomraning (1981) flux-limiter, given by

$$\lambda = \frac{1}{R} \left(\coth R - \frac{1}{R} \right), \quad (27)$$

$$R = \frac{|\nabla E_0|}{\kappa_{0R} E_0}. \quad (28)$$

However, our derivation is independent of this choice. Regardless of their exact functional form, all flux-limiters have the property that in an optically thick medium $\lambda \rightarrow 1/3$, thereby giving $\mathbf{F}_0 \rightarrow -[c/(3\kappa_{0R})]\nabla E_0$, the correct value for diffusion. In an optically thin medium, $\lambda \rightarrow (\kappa_{0R} E_0/|\nabla E_0|)\mathbf{n}_0$, where \mathbf{n}_0 is the unit vector antiparallel to ∇E_0 , so the flux approaches $\mathbf{F}_0 \rightarrow cE_0\mathbf{n}_0$, and the propagation speed of radiation is correctly limited to c .

For the Levermore & Pomraning flux-limiter we adopt, the corresponding approximate value for the radiation pressure tensor is (Levermore 1984)

$$\mathbf{P}_0 = \frac{E_0}{2} [(1 - R_2)\mathbf{I} + (3R_2 - 1)\mathbf{n}_0\mathbf{n}_0], \quad (29)$$

where \mathbf{I} is the identity tensor of rank 2 and

$$R_2 = \lambda + \lambda^2 R^2. \quad (30)$$

Physically, this approximation interpolates between the behavior in very optically thick regions, where $R_2 \rightarrow 1/3 + O(1/\tau^2)$, the radiation pressure is isotropic, and off-diagonal components vanish, and optically thin regions, where $R_2 \rightarrow 1$ and the radiation pressure tensor is zero orthogonal to \mathbf{n}_0 and E_0 parallel to it.

Note that for pure diffusion Mihalas & Weibel-Mihalas (1999) and Castor (2004) show that the pressure tensor reduces to $(E_0/3)\mathbf{I}$ plus off-diagonal elements of order β/τ or β^2 . Our approximation does not quite reproduce this, since in the diffusion limit, it gives $\mathbf{P}_0 = (E_0/3)\mathbf{I}$ plus off-diagonal elements of order τ^{-2} . We might therefore worry that, in the static diffusion regime

where $\beta \ll \tau^{-1}$, we have an incorrect term. However, examination of our final equations below shows that all terms arising from off-diagonal elements of \mathbf{P}_0 are smaller than order β in the static diffusion limit, so adopting the Levermore (1984) approximation for the pressure tensor does not introduce any incorrect terms at order β in the final equations.

To use the approximations from equations (26) and (29) to evaluate the radiation four-force, we must Lorentz transform them to express the radiation quantities in the lab frame. The Lorentz transforms for the energy, flux, and pressure to second order in v/c are (Mihalas & Weibel-Mihalas 1999)

$$E = E_0 + 2\frac{\mathbf{v} \cdot \mathbf{F}_0}{c^2} + \frac{1}{c^2} [v^2 E_0 + (\mathbf{v}\mathbf{v}) : \mathbf{P}_0], \quad (31)$$

$$\mathbf{F} = \mathbf{F}_0 + \mathbf{v}E_0 + \mathbf{v} \cdot \mathbf{P}_0 + \frac{1}{2c^2} [v^2 \mathbf{F}_0 + 3\mathbf{v}(\mathbf{v} \cdot \mathbf{F}_0)], \quad (32)$$

$$\mathbf{P} = \mathbf{P}_0 + \frac{\mathbf{v}\mathbf{F}_0 + \mathbf{F}_0\mathbf{v}}{c^2} + \frac{1}{c^2} [\mathbf{v}\mathbf{v}E_0 + \mathbf{v}(\mathbf{v} \cdot \mathbf{P}_0)]. \quad (33)$$

Note that in the expression for \mathbf{P} we have simplified the final term using the fact that \mathbf{P}_0 is a symmetric tensor.

Using the same scaling arguments we used to construct Table 1, we see that \mathbf{P} and \mathbf{P}_0 differ at order β in the streaming limit, at order β/τ for static diffusion, and at order β^2 for dynamic diffusion. Since this is below our accuracy goal, we need not distinguish \mathbf{P} and \mathbf{P}_0 . The same is true of E and E_0 . However, \mathbf{F} is different. In the comoving frame in an optically thick system, one is in the static diffusion regime, so $\mathbf{F}_0 \sim cE_0/\tau$. Since $\mathbf{v}E_0$ and $\mathbf{v} \cdot \mathbf{P}_0$ are of order βcE_0 and in dynamic diffusion $\beta \gg 1/\tau$, this means that $\mathbf{v}E_0$ and $\mathbf{v} \cdot \mathbf{P}_0$ are the dominant components of \mathbf{F} in dynamic diffusion and must therefore be retained. Thus,

$$\mathbf{F} = -\frac{c\lambda}{\kappa_{0R}} \nabla E + \mathbf{v}E + \mathbf{v} \cdot \mathbf{P}, \quad (34)$$

which is simply the rest-frame flux plus terms describing the advection of radiation enthalpy.

Substituting equation (29) with $\mathbf{P} = \mathbf{P}_0$ and equation (34) into the four-force density from equations (24) and (25) and continuing to retain terms to order v^2/c^2 gives

$$\begin{aligned} G^0 = & \kappa_{0P} \left(E - \frac{4\pi B}{c} \right) + \left(\frac{\lambda}{c} \right) \left(2\frac{\kappa_{0P}}{\kappa_{0R}} - 1 \right) \mathbf{v} \cdot \nabla E \\ & - \frac{\kappa_{0P}}{c^2} E \left[\frac{3 - R_2}{2} v^2 + \frac{3R_2 - 1}{2} (\mathbf{v} \cdot \mathbf{n})^2 \right] \\ & + \frac{1}{2} \left(\frac{v}{c} \right)^2 \kappa_{0P} \left(E - \frac{4\pi B}{c} \right), \end{aligned} \quad (35)$$

$$\begin{aligned} \mathbf{G} = & -\lambda \nabla E + \kappa_{0P} \frac{\mathbf{v}}{c} \left(E - \frac{4\pi B}{c} \right) - \frac{1}{2} \left(\frac{v}{c} \right)^2 \lambda \nabla E \\ & + 2\lambda \left(\frac{\kappa_{0P}}{\kappa_{0R}} - 1 \right) \frac{(\mathbf{v} \cdot \nabla E)\mathbf{v}}{c^2}, \end{aligned} \quad (36)$$

where \mathbf{n} is the unit vector antiparallel to ∇E . We again remind the reader that, although these equations contain terms of order β^2 , they are not truly accurate to order β^2 , because we did not retain all the β^2 when applying the Lorentz transform to the flux and pressure. However, these equations include all the terms that appear at the order of accuracy to which we are working,

TABLE 2
SCALINGS OF TERMS IN THE CONSERVATION EQUATIONS

Term	Equation	Streaming	Static Diffusion	Dynamic Diffusion
$\lambda \nabla E$	M	τ^*	1^*	1^*
$\kappa_{0P}(\mathbf{v}/c^2)(4\pi B - cE)$	M	$\beta\tau$	β/τ	$\beta^3\tau$
$(1/2)(v/c)^2 \lambda \nabla E$	M	$\beta^2\tau$	β^2	β^2
$2\lambda(\kappa_{0P}/\kappa_{0R} - 1)(\mathbf{v} \cdot \nabla E)\mathbf{v}/c^2$	M	$\beta^2\tau$	β^2	β^2
$\kappa_{0P}(4\pi B - cE)$	G and R	τ^*	$1/\tau^*$	$\beta^2\tau^*$
$\lambda(2\kappa_{0P}/\kappa_{0R} - 1)\mathbf{v} \cdot \nabla E$	G and R	$\beta\tau$	β	β^*
$\kappa_{0P}(v^2/c)[(3 - R_2)/2]E$	G and R	$\beta^2\tau$	$\beta^2\tau$	$\beta^2\tau^*$
$\kappa_{0P}[(\mathbf{v} \cdot \mathbf{n})^2/c][(3R_2 - 1)/2]E$	G and R	$\beta^2\tau$	β^2/τ	β^2/τ
$(1/2)(v/c)^2 \kappa_{0P}(cE - 4\pi B)$	G and R	$\beta^2\tau$	β^2/τ	$\beta^4\tau$
$\nabla \cdot [(c\lambda/\kappa_{0R})\nabla E]$	R	1^*	$1/\tau^*$	$1/\tau$
$\nabla \cdot \{[(3 - R_2)/2]\mathbf{v}E\}$	R	β	β	β^*
$\nabla \cdot \{[(3R_2 - 1)/2]\mathbf{v} \cdot (\mathbf{nn})E\}$	R	β	β/τ^2	β/τ^2

NOTES.—Col. (2): Which equation the term appears in, where M is for momentum eq. (37), G is for gas energy eq. (38), and R is for radiation energy eq. (39). Col. (3)–(5): All scalings are normalized to E/l for the momentum equation and cE/l for the energy equations. Scalings that are of leading order in each regime for each equation are denoted by an asterisk.

and by retaining terms of order β^2 , we guarantee that these terms will be preserved.

Inserting (G^0, \mathbf{G}) and the lab frame flux from equation (34) into the gas momentum and energy equations (7) and (8) and the radiation energy equation (9) and again retaining terms to order v^2/c^2 gives

$$\frac{\partial}{\partial t}(\rho\mathbf{v}) = -\nabla \cdot (\rho\mathbf{v}\mathbf{v}) - \nabla P - \lambda \nabla E - \kappa_{0P} \frac{v}{c^2} (4\pi B - cE) - \frac{1}{2} \left(\frac{v}{c}\right)^2 \lambda \nabla E + 2\lambda \left(\frac{\kappa_{0P}}{\kappa_{0R}} - 1\right) \frac{(\mathbf{v} \cdot \nabla E)\mathbf{v}}{c^2}, \quad (37)$$

$$\begin{aligned} \frac{\partial}{\partial t}(\rho e) = & -\nabla \cdot [(\rho e + P)\mathbf{v}] - \kappa_{0P}(4\pi B - cE) \\ & + \lambda \left(2\frac{\kappa_{0P}}{\kappa_{0R}} - 1\right) \mathbf{v} \cdot \nabla E \\ & - \frac{\kappa_{0P}}{c} E \left[\frac{3 - R_2}{2} v^2 + \frac{3R_2 - 1}{2} (\mathbf{v} \cdot \mathbf{n})^2 \right] \\ & - \frac{1}{2} \left(\frac{v}{c}\right)^2 \kappa_{0P}(4\pi B - cE), \end{aligned} \quad (38)$$

$$\begin{aligned} \frac{\partial}{\partial t}E = & \nabla \cdot \left(\frac{c\lambda}{\kappa_{0R}} \nabla E \right) + \kappa_{0P}(4\pi B - cE) \\ & - \lambda \left(2\frac{\kappa_{0P}}{\kappa_{0R}} - 1\right) \mathbf{v} \cdot \nabla E \\ & + \frac{\kappa_{0P}}{c} E \left[\frac{3 - R_2}{2} v^2 + \frac{3R_2 - 1}{2} (\mathbf{v} \cdot \mathbf{n})^2 \right] \\ & + \frac{1}{2} \left(\frac{v}{c}\right)^2 \kappa_{0P}(4\pi B - cE) \\ & - \nabla \cdot \left[\frac{3 - R_2}{2} \mathbf{v}E + \frac{3R_2 - 1}{2} \mathbf{v} \cdot (\mathbf{nn})E \right]. \end{aligned} \quad (39)$$

At this point we construct Table 2, showing the scalings of the radiation terms to see which must be retained and which are superfluous. In constructing Table 2, we take spatial derivatives to be of characteristic scaling $1/l$, i.e., we assume that radiation quantities vary on a size scale of the system, rather than over a size scale of the photon mean free path. In the streaming limit, $\lambda \sim \tau$ and $R_2 \sim 1 + O(\tau)$. In the diffusion limit, $\lambda \sim 1/3$ and $R_2 \sim 1/3 + O(\tau^{-2})$.

Using Table 2 to drop all terms that are not significant at leading order in any regime, we arrive at our final equations,

$$\frac{\partial}{\partial t}(\rho\mathbf{v}) = -\nabla \cdot (\rho\mathbf{v}\mathbf{v}) - \nabla P - \lambda \nabla E, \quad (40)$$

$$\begin{aligned} \frac{\partial}{\partial t}(\rho e) = & -\nabla \cdot [(\rho e + P)\mathbf{v}] - \kappa_{0P}(4\pi B - cE) \\ & + \lambda \left(2\frac{\kappa_{0P}}{\kappa_{0R}} - 1\right) \mathbf{v} \cdot \nabla E - \frac{3 - R_2}{2} \kappa_{0P} \frac{v^2}{c} E, \end{aligned} \quad (41)$$

$$\begin{aligned} \frac{\partial}{\partial t}E = & \nabla \cdot \left(\frac{c\lambda}{\kappa_{0R}} \nabla E \right) + \kappa_{0P}(4\pi B - cE) \\ & - \lambda \left(2\frac{\kappa_{0P}}{\kappa_{0R}} - 1\right) \mathbf{v} \cdot \nabla E \\ & + \frac{3 - R_2}{2} \kappa_{0P} \frac{v^2}{c} E - \nabla \cdot \left(\frac{3 - R_2}{2} \mathbf{v}E \right). \end{aligned} \quad (42)$$

These represent, respectively, the equations of momentum conservation for the gas, energy conservation for the gas, and energy conservation for the radiation field, which, together with mass conservation equation (6), fully describe the system under the approximations we have adopted. They are accurate and consistent to leading order in the streaming and dynamic diffusion limits. They are accurate to first order in β in the static diffusion limit, since we have had to retain all order β terms in this limit, because they are of leading order in dynamic diffusion problems. In addition, note that if in a given problem one never encounters the dynamic diffusion regime, it is possible to drop more terms, as we discuss in § 4.

The equations are easy to understand intuitively. The term $-\lambda \nabla E$ in momentum equation (40) simply represents the radiation force $\kappa_{0R}\mathbf{F}/c$, neglecting distinctions between the co-moving and laboratory frames which are smaller than leading order in this equation. Similarly, the terms $\pm \kappa_{0P}(4\pi B - cE)$ and $\pm \lambda(2\kappa_{0P}/\kappa_{0R} - 1)\mathbf{v} \cdot \nabla E$ in the two energy equations (41) and (42) represent radiation absorbed minus radiation emitted by the gas and the work done by the radiation field as it diffuses through the gas, respectively. The factor $(2\kappa_{0P}/\kappa_{0R} - 1)$ arises because the term contains contributions both from the Newtonian work and from a relativistically induced mismatch between emission and absorption. The term proportional to $\kappa_{0P}E/c$ represents another relativistic correction to the work, this one arising from

boosting of the flux between the lab and comoving frames. In radiation energy equation (42), the first term on the left-hand side is the divergence of the radiation flux, i.e., the rate at which radiation diffuses, and the last term on the right-hand side represents advection of the radiation enthalpy $E + \mathbf{P}$ by the gas.

It is also worth noting that equations (38) and (39) are manifestly energy conserving, since every term in one equation either has an obvious counterpart in the other with opposite sign or is clearly an advection. In contrast, momentum equation (40) is not manifestly momentum conserving, since there is a force term $-\lambda \nabla E$ with no equal and opposite counterpart. This nonconservation of momentum is an inevitable side effect of using the flux-limited diffusion approximation, since this approximation amounts to allowing the radiation field to transfer momentum to the gas without explicitly tracking the momentum of the radiation field and the corresponding transfer from gas to radiation.

3. THE IMPORTANCE OF HIGHER ORDER TERMS

Our dynamical equations result from retaining at least some terms that are formally of order β^2 . Even though our analysis shows that these terms can be the leading ones present, due to cancellations of lower order terms, one might legitimately ask whether they are ever physically significant. In § 3.1 we address this question by comparing our equations to those that result from lower order treatments. In § 3.2 we also compare our equations with those generally used in comoving-frame formulations of radiation hydrodynamics.

To make our work in this section more transparent and since we are more interested in physical intuition than rigorous derivation here, we specialize to the diffusion regime in gray materials. Thus, we set $\lambda = R_2 = 1/3$ and $\kappa_{0P} = \kappa_{0R} = \kappa_0$. A more general analysis produces the same conclusions, but is more mathematically cumbersome. We also focus on the radiation energy equation, since all the terms that appear in the gas energy equation also appear in it and because there are no higher order terms present in the momentum equation. Under these assumptions, our radiation energy equation (42) becomes

$$\frac{\partial}{\partial t} E = \nabla \cdot \left(\frac{c}{3\kappa_0} \nabla E \right) + \kappa_0(4\pi B - cE) - \frac{4}{3} \nabla \cdot (\mathbf{v}E) - \frac{1}{3} \mathbf{v} \cdot \nabla E + \frac{4}{3} \kappa_0 \frac{v^2}{c} E. \quad (43)$$

3.1. Comparison to Lower Order Equations

A common approach in radiation hydrodynamic problems is to expand the equations in β , rather than in both β and τ as we have done, and to drop at least some terms that are of order β^2 in every regime (e.g., Mihalas & Weibel-Mihalas 1999). To determine how equations derived in this manner compare to our higher order treatment, we compare our simplified energy equation (43) to the corresponding equation one would obtain by following this procedure with equation (42). This resulting energy equation is

$$\frac{\partial}{\partial t} E = \nabla \cdot \left(\frac{c}{3\kappa_0} \nabla E \right) + \kappa_0(4\pi B - cE) - \frac{4}{3} \nabla \cdot (\mathbf{v}E) - \frac{1}{3} \mathbf{v} \cdot \nabla E. \quad (44)$$

It is important to caution at this point that, as we show below, equation (44) is not accurate to leading order in at least some cases and should not be used for computations unless one care-

fully checks that the missing terms never become important in the regime covered by the computation.

Compared to energy equation (43) that we obtain by retaining all leading-order terms in β and τ , equation (44) is missing the term $(4/3)\kappa_0 v^2 E/c$. If we think of the flux as having two parts, a “diffusion” part proportional to ∇E that comes from radiation diffusion in the comoving frame and a “relativistic” part proportional to $\mathbf{v}E + \mathbf{v} \cdot \mathbf{P}$ that comes from the Lorentz transformation between lab and comoving frames, then it is natural to describe the $\mathbf{v} \cdot \nabla E$ term as the “diffusion work” arising from the combination of the diffusion flux and the post-Newtonian emission-absorption mismatch (as discussed in § 2.2) and the $\kappa_0 v^2 E/c$ term as the “relativistic work” arising from the relativistic flux. The presence or absence of this relativistic work term is the difference between our leading-order accurate equation and the equation one would derive by dropping β^2 terms. Analyzing when, if ever, this term is physically important lets us identify in which situations a lower order treatment may be inadequate.

If we use Table 2 to compare the relativistic work term to the emission/absorption term, we find that $(\kappa_0 v^2 E/c)/[\kappa_0(4\pi B - cE)]$ is of order $\beta^2 \tau^2$ for static diffusion and of order unity for dynamic diffusion. Thus, the term is never important in a static diffusion problem, but is always important for a nonuniform, nonequilibrium dynamic diffusion problem system. We add the caveats about nonuniformity and time dependence, because in a system where there is no radiation-gas energy exchange, the relativistic work term will be small due to a cancellation. The example in the Appendix shows that in an equilibrium, uniform medium, the terms $\kappa_0(4\pi B - cE)$ and $(4/3)\kappa_0 v^2 E/c$ cancel exactly at orders up to β^2 . We expect any system where variations occur on a scale for which $\beta\tau \gg 1$ to resemble such a uniform, equilibrium medium, and thus, we do not expect the term $(4/3)\kappa_0 v^2 E/c$ to be important in such a system.

That said, there is still clearly a problem with omitting the relativistic work term in a system where $\beta\tau \sim 1$. In this case, Table 2 implies that *every* term on the right-hand side is roughly equally important regardless of whether we use the static or dynamic diffusion scalings. To illustrate this point, consider a radiation-dominated shock. The width of such a shock is set by the balance between radiation diffusing upstream from the hot postshock region into the cold preshock region and advection of the radiation back downstream by the preshock gas. This condition requires that $\beta\tau \sim 1$ across the shock (Mihalas & Weibel-Mihalas 1999), so its width $w \sim \lambda_p/\beta$. Since E changes by of order unity across this distance, its spatial derivative is of order $\nabla E \sim E/w \sim (\beta/\lambda_p)E$. Applying this to equation (43), we find that each term on the right-hand side is of order $\beta^2(c/\lambda_p)E$. Since the terms like $-(4/3)\nabla \cdot (\mathbf{v}E)$ describing advection and $\nabla \cdot [c/(3\kappa_0)\nabla E]$ describing diffusion are obviously important in the structure of the shock, causing order unity changes in E , and the relativistic work term is comparable, it follows that the relativistic work term is equally important. One can obtain the correct structure within a radiation-dominated shock only by retaining the relativistic work term.

An interesting point to note here is that omitting the relativistic work term will not produce errors upstream or downstream of a shock, because $\beta\tau \gg 1$ in these regions. Furthermore, the jump conditions across a shock should be correct. The omitted term affects radiation-gas energy exchange, not total energy conservation, and all that is required to get the correct jump conditions are conservation of mass and energy plus correct computation of the upstream and downstream radiation pressures. The lower order treatment will therefore only make errors within the shock.

Whether this is physically important or it is sufficient to get the jump conditions correct depends on whether one is concerned with structures on scales for which $\beta\tau \sim 1$. An astrophysical example of a system where one does care about structures on this scale is a radiation-dominated accretion disk subject to photon bubble instability (Turner et al. 2003). Such disks are in the dynamic diffusion regime over the entire disk, but photon bubbles form on small scales within them, and individual bubbles can have $\beta\tau \sim 1$ across them.

3.2. Comparison to Comoving-frame Formulations

Many popular numerical treatments of radiation hydrodynamics (e.g., Turner & Stone 2001; Whitehouse & Bate 2004; Hayes et al. 2006) use a comoving formulation of the equations rather than our mixed-frame formulation. It is therefore useful to compare our equations to the standard comoving-frame equations. In the comoving formulation, the evolution equation for the radiation field is usually the first law of thermodynamics for the comoving radiation field (Mihalas & Klein 1982),

$$\rho \frac{D}{Dt} \left(\frac{E_0}{\rho} \right) + \mathbf{P}_0 : (\nabla \mathbf{v}) = \kappa_0(4\pi B - cE_0) - \nabla \cdot \mathbf{F}_0. \quad (45)$$

This equation is accurate to first order in β in the sense that it contains all the correct leading-order terms and all terms that are smaller than them by order β or less.

To compare this to our mixed-frame radiation energy equation (42), we replace the comoving-frame energy E_0 in equation (45) with the lab frame energy E using the Lorentz transformation from equation (31) and retain all terms that are of leading order in any regime. In practice, this means that we set $E_0 = E$ inside the time derivative, since the difference between E and E_0 is at most β/τ or β^2 for static or dynamic diffusion. However, when replacing E_0 with E in the heating/cooling term $4\pi B - cE_0$, we must retain all the terms in equation (31), because the leading term $4\pi B - cE$ is itself only of order τ^{-2} or β^2 relative to E , so the difference between E and E_0 can be of leading order.² This gives a transformed equation

$$\rho \frac{D}{Dt} \left(\frac{E}{\rho} \right) + \mathbf{P}_0 : (\nabla \mathbf{v}) = \kappa_0(4\pi B - cE) - \nabla \cdot \mathbf{F}_0 + 2\kappa_0 \frac{\mathbf{v} \cdot \mathbf{F}_0}{c} + \frac{\kappa_0}{c} [v^2 E + (\mathbf{v} \mathbf{v}) : \mathbf{P}_0]. \quad (46)$$

If we now adopt the diffusion approximation $\mathbf{F}_0 = -c/(3\kappa_0)\nabla E_0$ and $\mathbf{P}_0 = (1/3)E_0\mathbf{I}$, use the Lorentz transformation to replace E_0 with E throughout, and again only retain terms that are of leading order in some regime, then it is easy to verify that equation (46) reduces to equation (43). Thus, our evolution equation is equivalent to the comoving-frame first law of thermodynamics for the radiation field, provided that one retains all the leading-order terms with respect to β and τ , including some that are of order β^2 , when evaluating the Lorentz transformation.

While the equations are equivalent, the mixed-frame formulation has two important advantages over the comoving-frame formulation when it comes to practical computation. First, we

are able to write the equations in a manner that allows a numerical solution algorithm to conserve total energy to machine accuracy. We present such an algorithm in § 4. In contrast, it is not possible to write a conservative update algorithm using the comoving-frame equations. The reason for this is that a conserved total energy only exists in an inertial frame, and for a fluid whose velocity is not a constant in space and time, the comoving frame is not inertial. The lack of a conserved energy is a serious drawback to comoving-frame formulations.

A second advantage of the mixed-frame formulation is that it is far more suited to implementation in codes with dynamically modified grid structures such as adaptive mesh refinement methods. Since the radiation energy is a conserved quantity, it is obvious how to refine or coarsen it in a conservative manner. On the other hand, there is no obviously correct method for refining or coarsening the comoving-frame energy density, because it will not even be defined in the same reference frames before and after the refinement procedure.

4. AN OPTIMIZED ALGORITHM FOR STATIC DIFFUSION RADIATION HYDRODYNAMICS

4.1. Operator Splitting

Our analysis shows that for static diffusion, the terms involving diffusion and emission minus absorption of radiation always dominate over those involving radiation work and advection. In addition, some terms are always smaller than order β . This suggests an opportunity for a significant algorithmic improvement over earlier approaches while still retaining order β accuracy in the solution. In a simulation, one must update terms for the radiation field implicitly, because otherwise stability requirements limit the update time step to values comparable to the light crossing time of a cell. Standard approaches (e.g., Turner & Stone 2001; Whitehouse & Bate 2004; Whitehouse et al. 2005; Hayes et al. 2006) therefore update all terms involving radiation implicitly except the advection term and the radiation force term in the gas momentum equation.

However, implicit updates are computationally expensive, so the simpler the terms to be updated implicitly can be made, the simpler the algorithm will be to code and the faster it will run. Since the work and advection terms are nondominant, we can produce a perfectly stable algorithm without treating them implicitly. Even if this treatment introduces numerically unstable modes in the work or advection terms, they will not grow because the radiation diffusion and emission/absorption terms, which are far larger, will smooth them away each time step.

For the case of static diffusion, we therefore adopt the order v/c equations (6) and (40) for mass and momentum conservation. For our energy equations, we adopt equations (41) and (42), but drop terms that are smaller than order β for static diffusion. This gives

$$\begin{aligned} \frac{\partial}{\partial t}(\rho e) = & -\nabla \cdot [(\rho e + P)\mathbf{v}] - \kappa_{0P}(4\pi B - cE) \\ & + \lambda \left(2 \frac{\kappa_{0P}}{\kappa_{0R}} - 1 \right) \mathbf{v} \cdot \nabla E, \end{aligned} \quad (47)$$

$$\begin{aligned} \frac{\partial}{\partial t} E = & \nabla \cdot \left(\frac{c\lambda}{\kappa_{0R}} \nabla E \right) + \kappa_{0P}(4\pi B - cE) \\ & - \lambda \left(2 \frac{\kappa_{0P}}{\kappa_{0R}} - 1 \right) \mathbf{v} \cdot \nabla E - \nabla \cdot \left(\frac{3 - R_2}{2} \mathbf{v} E \right). \end{aligned} \quad (48)$$

To solve these, we operator split the diffusion and emission/absorption terms, which we treat implicitly, from the work and

² Note that our need to retain difference between E and E_0 here is different from the situation when we first applied the Lorentz transformation to derive eqs. (35) and (36). In that case we did not need to retain the distinction between E and E_0 , because in deriving eqs. (35) and (36), there were no terms involving E_0 explicitly. Instead, E_0 appeared only implicitly, as part of the flux \mathbf{F} , and non-leading-order corrections to \mathbf{F} are not of leading order in any regime. In contrast, E_0 does appear explicitly in eq. (45).

advection terms, which we treat explicitly. To do this, we write our gas/radiation state as

$$\mathbf{q} = \begin{pmatrix} \rho \\ \rho \mathbf{v} \\ \rho e \\ E \end{pmatrix} \quad (49)$$

and our evolution equations as

$$\frac{\partial \mathbf{q}}{\partial t} = \mathbf{f}_{\text{e-nr}} + \mathbf{f}_{\text{e-rad}} + \mathbf{f}_{\text{i-rad}}, \quad (50)$$

where we have broken our right-hand side up into nonradiative terms to be handled explicitly,

$$\mathbf{f}_{\text{e-nr}} = \begin{pmatrix} -\nabla \cdot (\rho \mathbf{v}) \\ -\nabla \cdot (\rho \mathbf{v} \mathbf{v}) - \nabla P \\ -\nabla \cdot [(\rho e + P) \mathbf{v}] \\ 0 \end{pmatrix}, \quad (51)$$

radiative terms to be handled explicitly,

$$\mathbf{f}_{\text{e-rad}} = \begin{pmatrix} 0 \\ -\lambda \nabla E \\ \lambda \left(2 \frac{\kappa_{0P}}{\kappa_{0R}} - 1 \right) \mathbf{v} \cdot \nabla E \\ -\lambda \left(2 \frac{\kappa_{0P}}{\kappa_{0R}} - 1 \right) \mathbf{v} \cdot \nabla E - \nabla \cdot \left(\frac{3 - R_2}{2} \mathbf{v} E \right) \end{pmatrix}, \quad (52)$$

and radiative terms that must be handled implicitly,

$$\mathbf{f}_{\text{i-rad}} = \begin{pmatrix} 0 \\ 0 \\ -\kappa_{0P}(4\pi B - cE) \\ \nabla \cdot \left(\frac{c\lambda}{\kappa_{0R}} \nabla E \right) + \kappa_{0P}(4\pi B - cE) \end{pmatrix}. \quad (53)$$

4.2. Update Scheme

For each update cycle, we start with the state \mathbf{q}^n at the old time. We first perform an implicit update to the radiation and gas energy densities using $\mathbf{f}_{\text{i-rad}}$. Any number of methods are possible for this. For our implementation of this algorithm in the Orion adaptive mesh refinement (AMR) code, we use the method of Howell & Greenough (2003) which we do not discuss in detail here. To summarize, the algorithm involves writing the equations using second-order accurate spatial discretization and a time discretization that limits to backward Euler for large values of $\partial E / \partial t$ (to guarantee stability) and to Crank-Nicolson when $\partial E / \partial t$ is small (to achieve second-order time accuracy). This yields a matrix equation for the radiation and gas energy densities at the new time, which can be solved on both individual grids and over a hierarchy of nested grids (as is necessary for AMR) using standard multigrid techniques. The output of this procedure is an intermediate state $\mathbf{q}^{n,*}$ which has been updated for $\mathbf{f}_{\text{i-rad}}$.

Once the implicit update is done, we compute the ordinary hydrodynamic update. As with the implicit update, this can be done using the hydrodynamics method of one's choice. For our implementation, we use the Godunov method described by

Truelove et al. (1998), Klein (1999), and Fisher (2002). This update gives us $\mathbf{q}^{n,\dagger}$, the state updated for $\mathbf{f}_{\text{i-rad}}$ and $\mathbf{f}_{\text{e-nr}}$. The only modification we make to the standard update algorithm is to include a radiation pressure term in the effective sound speed used to compute the Courant condition. Thus, we take

$$c_{\text{eff}} = \sqrt{\frac{\gamma P + (4/9)E(1 - e^{-\kappa_{0R}\Delta x})}{\rho}} \quad (54)$$

and set the time step to

$$\Delta t = C \frac{\Delta x}{\max(|\mathbf{v}| + c_{\text{eff}})}, \quad (55)$$

where γ is the ratio of specific heats for the gas, C is the Courant factor (usually 0.5), and the maximum is evaluated over all cells. For AMR, this condition is applied independently on each level l , and the time step is set using the values of Δt^l in the standard AMR manner (e.g., Klein 1999). The factor $(1 - e^{-\kappa_{0R}\Delta x})$ gives us a means of interpolating between optically thick cells, where radiation pressure contributes to the restoring force and thus increases the effective signal speed, and optically thin cells, where radiation does not provide any pressure.

Finally, we compute the force and advection terms in $\mathbf{f}_{\text{e-rad}}$. In our implementation we compute all of these at cell centers using second-order centered differences. For ∇E this is

$$(\nabla E)_{i,j,k}^{n,*} = \left(\frac{E_{i+1,j,k}^{n,*} - E_{i-1,j,k}^{n,*}}{2\Delta x}, \frac{E_{i,j+1,k}^{n,*} - E_{i,j-1,k}^{n,*}}{2\Delta y}, \frac{E_{i,j,k+1}^{n,*} - E_{i,j,k-1}^{n,*}}{2\Delta z} \right). \quad (56)$$

Other derivatives are computed in an analogous manner. We then find the new state by

$$\mathbf{q}^{n+1} = \mathbf{q}^{n,\dagger} + \mathbf{f}_{\text{e-rad}} \Delta t. \quad (57)$$

This update is manifestly only first-order accurate in time for the explicit radiation terms, but there is no point in using a more complex update, because our operator splitting of some of the radiation terms means that we are performing our explicit update using a time-advanced radiation field, rather than the field at a half-time step. (Truelove et al. [1998] show that one can avoid this problem for gravitational body forces, because the potential is linear in the density, so it is possible to derive the half-time step potential from the whole time step states. No such fortuitous coincidence occurs for the radiation field.) This necessarily limits us to first-order accuracy in time for the terms we treat explicitly. However, since these terms are always small compared to the dominant radiation terms, the overall scheme should still be closer to second order than first order in accuracy.

4.3. Advantages and Limitations of the Method

Our algorithm has two significant advantages in comparison to other approaches, in particular those based on comoving-frame formulations of the equations (e.g., Turner & Stone 2001; Whitehouse et al. 2005; Hayes et al. 2006). In any of these approaches, since the radiation work terms are included in the implicit update, one must solve an implicit quartic equation arising from the combination of the terms $\kappa_{0P}(4\pi B - cE)$ and $\mathbf{P} \cdot \nabla \mathbf{v}$.

This can be done either at the same time one is iterating to update the flux divergence term $\nabla \cdot \mathbf{F}$ (Whitehouse et al. 2005) or in a separate iteration to be done once the iterative solver for the flux divergence update is complete (Turner & Stone 2001; Hayes et al. 2006). In contrast, since our iterative update involves only $\kappa_{0P}(4\pi B - cE)$ and $\nabla \cdot \mathbf{F}$, using the Howell & Greenough (2003) algorithm we can linearize the equations and never need to solve a quartic, leading to a simpler update algorithm and a faster iteration step. Moreover, by using the Howell & Greenough (2003) time centering, we obtain second-order accuracy in time whenever E is changing slowly, as opposed to the backward Euler differencing of Turner & Stone (2001), Whitehouse et al. (2005), and Hayes et al. (2006) which is always first-order accurate in time. Thus, our algorithm provides a faster and simpler approach than the standard one.

A second advantage of our update scheme is that it retains the total energy-conserving character of the underlying equations. In each of the update steps involving radiation, for f_{e-rad} and f_{i-rad} , the nonadvective update terms in the radiation and gas energy equations are equal and opposite. Thus, it is trivial to write the update scheme so that it conserves total energy to machine precision. This property is particularly important for turbulent flows with large radiation energy gradients, such as those that occur in massive star formation (e.g., Krumholz et al. 2007), because numerical nonconservation is likely to be exacerbated by the presence of these features. In contrast, in comoving-frame formalisms such as those of Turner & Stone (2001), Whitehouse & Bate (2004), and Hayes et al. (2006), the exchange terms in their gas and radiation energy equations are not symmetric. As a result, their update schemes do not conserve total energy exactly. The underlying physical reason for this asymmetry is that total energy is conserved only in inertial frames such as the lab frame; it is not conserved in the noninertial comoving frame. For this reason, there is no easy way to write a conservative update scheme from a comoving formulation.

Our algorithm also has two significant limitations, one obvious and one subtle. The obvious limit is that our algorithm is only applicable for static diffusion problems. For dynamic diffusion problems, e.g., stellar interiors or radiation-dominated shocks, our scheme is unstable unless an appropriately small time step is used. Whether this instability is due to the explicit advection term, the explicit work term, or both is not clear. Since codes such as ZEUS (Hayes et al. 2006) treat the advection explicitly without instability, however, it seems likely that the work term is the culprit. Regardless of the cause, even if we were to use a time step small enough to guarantee stability, since the work and advection terms can be comparable to or larger than the diffusion and heating/cooling terms for dynamic diffusion, an algorithm that treats all the terms implicitly or all explicitly, rather than our mix, is likely to be more accurate.

The subtle limitation is in our treatment of the hydrodynamics. We perform the hydrodynamic update using a Riemann solver unmodified for the presence of radiation force, work, and heating and cooling terms. These terms should change the characteristic velocities of the wave families in ways that depend on the radiation hydrodynamic regime of the system. For example, in optically thick systems we should have a radiation-acoustic mode rather than a simple sound wave, and in optically thin systems where the radiation timescale is short compared to the mechanical timescale, a gas may act as if it were isothermal even if it has $\gamma \neq 1$. In some cases, failure to modify the Riemann solver appropriately for these effects may produce substantial errors, including a reduction in the order of accuracy of the method from second to first (Pember 1993; Lowrie & Morel 2001; Miniati &

Colella 2007). The severity of these effects for a given problem depends on the degree of stiffness of the radiation source terms. It should also be noted that the other radiation diffusion methods most commonly used for three-dimensional problems also suffer from this defect, so this is not a comparative disadvantage of our method relative to others.

5. TESTS OF THE STATIC DIFFUSION ALGORITHM

Here we describe five tests of our static diffusion algorithm, done using our implementation of the algorithm in the Orion AMR code, various aspects of which are described in detail by Puckett & Saltzman (1992) multifluid hydrodynamics, Truelove et al. (1998) hydrodynamics and gravity, Klein (1999) hydrodynamics and gravity, Fisher (2002) gravity, Howell & Greenough (2003) radiation transport, Krumholz et al. (2004) sink particles, and Crockett et al. (2005) magnetohydrodynamics. For all of these tests we use a single fluid with no magnetic fields and no self-gravity.

5.1. Nonequilibrium Marshak Wave

As an initial check of the gas-radiation energy exchange in our code in a case when radiation pressure is not significant and the gas is at rest, we simulate the nonequilibrium Marshak wave problem. In this problem, a zero-temperature, motionless, gaseous medium occupying all space at $z > 0$ is subject to a constant radiation flux $F_{inc} \hat{z}$ incident on its surface at $z = 0$. The gas is held stationary, appropriate for early times before hydrodynamic motions become significant. The medium is gray, with opacity $\kappa_{0R} = \kappa_{0P} = \kappa$, and the constant-volume specific heat capacity of the gas is taken to have the same T^3 dependence as that of the radiation, i.e., $c_v = [\partial(e - v^2/2)/\partial T_g]_v = \alpha T_g^3$, where T_g is the gas temperature. The gas is not assumed to be in thermal equilibrium with the radiation field, so the gas and radiation temperatures may be different.

Su & Olson (1996) give a semianalytic solution to the time-dependent behavior of the radiation energy density $E(z, t)$ and gas temperature $T_g(z, t)$ for this problem. They introduce the dimensionless position and time variables $x \equiv \sqrt{3}\kappa z$ and $\tau \equiv (4a_R c \kappa / \alpha) t$ and the “retardation” parameter $\epsilon \equiv 4a_R / \alpha$, and show that the dimensionless radiation energy density

$$u(x, \tau) \equiv \left(\frac{c}{4}\right) \left[\frac{E(z, t)}{F_{inc}}\right] \quad (58)$$

$$= 1 - \frac{2\sqrt{3}}{\pi} \int_0^1 d\eta e^{-\tau\eta^2} \left\{ \frac{\sin[x\gamma_1(\eta) + \theta_1(\eta)]}{\eta\sqrt{3 + 4\gamma_1^2(\eta)}} \right\} - \frac{\sqrt{3}}{\pi} e^{-\tau} \int_0^1 d\eta e^{-\tau/(\epsilon\eta)} \left\{ \frac{\sin[x\gamma_2(\eta) + \theta_2(\eta)]}{\eta(1 + \epsilon\eta)\sqrt{3 + 4\gamma_2^2(\eta)}} \right\}, \quad (59)$$

where

$$\gamma_1(\eta) = \eta \sqrt{\epsilon + \frac{1}{1 - \eta^2}}, \quad (60)$$

$$\gamma_2(\eta) = \sqrt{(1 - \eta) \left(\epsilon + \frac{1}{\eta} \right)}, \quad (61)$$

$$\theta_n(\eta) = \cos^{-1} \sqrt{\frac{3}{3 + 4\gamma_n^2(\eta)}}. \quad (62)$$

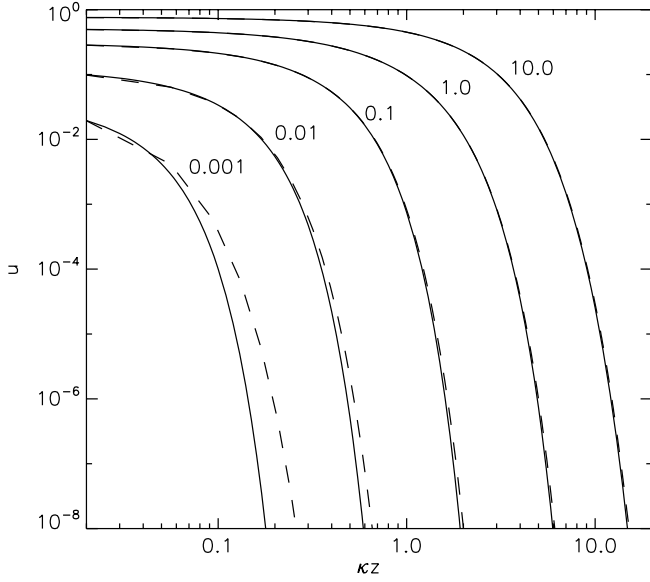


FIG. 1.—Dimensionless radiation energy density u vs. optical depth κz at a series of times τ . We show the semianalytic solution (solid lines) and the solution computed with Orion (dashed lines). The value of the dimensionless time τ is indicated by each curve.

The dimensionless gas energy density is

$$v(x, \tau) \equiv \left(\frac{c}{4}\right) \left[\frac{a_R T_g^4(z, t)}{F_{\text{inc}}} \right] \quad (63)$$

$$= u(x, \tau) - \frac{2\sqrt{3}}{\pi} \int_0^1 d\eta e^{-\tau(1-\eta^2)} \left\{ \frac{\sin[x\gamma_3(\eta) + \theta_3(\eta)]}{\sqrt{4 - \eta^2 + 4\epsilon\eta^2(1 - \eta^2)}} \right\} \\ + \frac{\sqrt{3}}{\pi} e^{-\tau} \int_0^1 d\eta e^{-\tau/(\epsilon\eta)} \left\{ \frac{\sin[x\gamma_2(\eta) + \theta_2(\eta)]}{\eta\sqrt{3 + 4\epsilon\eta^2(\eta)}} \right\}, \quad (64)$$

where

$$\gamma_3(\eta) = \sqrt{(1 - \eta^2) \left(\epsilon + \frac{1}{\eta^2} \right)}. \quad (65)$$

Numerical evaluation of the integrals from equations (59) and (64) for u and v is not trivial, because the integrands perform an infinite number of oscillations about zero as $\eta \rightarrow 0$. Correct computation of the result when τ is small and x is large requires careful numerical analysis to ensure that the positive and negative contributions cancel properly (J. Bolstad 2007, in preparation).

We compare the properly computed semianalytic results for u and v to a calculation performed with Orion using $\kappa = 1 \text{ cm}^{-1}$ and $\alpha = 32a_R/c$ (so $\epsilon = 0.5$). The computational domain goes from 0 to 15 cm (and thus to an optical depth $\kappa z = 15$) and is resolved by 100 equally sized cells. For this test, since we are comparing to a pure diffusion result, we set the flux-limiter $\lambda = 1/3$ everywhere.

Figures 1 and 2 compare the semianalytic dimensionless radiation and gas energy densities with the values computed by Orion. At $\tau = 0.001$ the agreement is fairly poor due to low numerical resolution, since the wave only reaches an optical depth of $\kappa z \sim 0.2$ and $\kappa z = 0.15$ is the size of an individual computational cell. However, at later times when the wave is resolved by a reasonable number of cells, the agreement between the code result and the semianalytic solution is excellent.

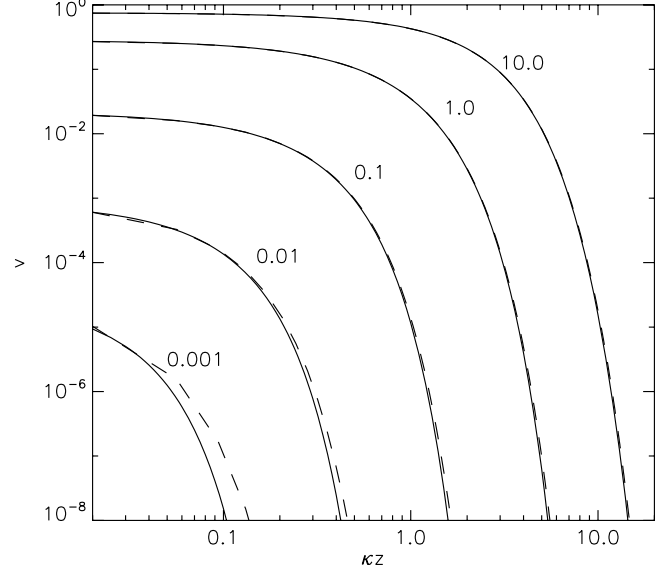


FIG. 2.—Same as Fig. 1, but for the dimensionless gas energy density v .

5.2. Radiating Blast Wave

We next compare to a test problem in which the gas is not at rest: a Sedov-type blast wave with radiation diffusion. Reinicke & Meyer-ter-Vehn (1991) gave the first similarity solution to the problem of a point explosion with heat conduction, and following Shestakov (1999) and Shestakov & Greenough (2001), we can adapt this solution to the case of a point explosion with radiation diffusion. This tests our code's ability to follow coupled radiation hydrodynamics in cases where radiation pressure is small.

We first summarize the semianalytic solution. Consider an $n = 3$ dimensional space filled with an adiabatic gas with equation of state $P = (\gamma - 1)\rho e \equiv \Gamma\rho T$, where Γ is the gas constant. The Planck mean opacity κ_{0P} of the gas is very high, so the gas and radiation temperatures are always equal. The Rosseland mean opacity has a power-law form $\kappa_{0R} = \kappa_{0R,0}\rho^m T^{-n}$, and we assume that it is always high enough to place us in the diffusion regime, so $\lambda = 1/3$. Note that the choice of $-n = -3$ as the exponent of the opacity power law is a necessary condition for applying the Reinicke & Meyer-ter-Vehn (1991) conduction solution to our radiation diffusion problem. Moreover, the similarity solution does not include radiation energy density or pressure, so we consider only temperatures for which the gas energy density and pressure greatly exceed the radiation energy density and pressure, i.e., $\rho e \gg a_R T^4$.

Under the assumptions described above, we can rewrite the gas and radiation energy equations (41) and (42) as a single conduction-type equation for the temperature,

$$\rho c_v \frac{\partial}{\partial t} T = \nabla \cdot (\chi_0 \rho^a T^b \nabla T), \quad (66)$$

where $c_v = \partial e / \partial T = \Gamma / (\gamma - 1)$ is the constant-volume specific heat of the gas, $\chi_0 = 4ca_R / (3\kappa_{0R,0})$, $a = -m$, and $b = n + 3$. This equation has the same form as the conduction equation considered by Reinicke & Meyer-ter-Vehn (1991).

Consider now a point explosion at the origin of a spherically symmetric region with an initial power-law density distribution $\rho(r, t = 0) = g_0 r^{-k_\rho}$. Initially, the gas temperature T and pressure P are negligible. The explosion occurs at the origin at time zero, so the initial gas energy density is $(\rho e)(r, t = 0) = E_0 \delta(\mathbf{r})$.

Reinicke & Meyer-ter-Vehn (1991) show that if the initial density profile has a power-law index

$$k_\rho = \frac{(2b-1)n+2}{2b-2a+1}, \quad (67)$$

then one can obtain a similarity solution via the change of variables

$$\xi = \frac{r}{\zeta t^\alpha}, \quad (68)$$

$$G(\xi) = \frac{\rho(r, t)}{g_0 r^{-k_\rho}}, \quad (69)$$

$$U(\xi) = v(r, t) \frac{t}{\alpha r}, \quad (70)$$

$$\Theta(\xi) = T(r, t) \Gamma \left(\frac{\alpha r}{t} \right)^2, \quad (71)$$

where ξ , $G(\xi)$, $U(\xi)$, and $\Theta(\xi)$ are the dimensionless distance, density, velocity, and temperature, respectively,

$$\alpha = \frac{2b-2a+1}{2b-(n+2)a+n}, \quad (72)$$

and ζ is a constant with units of (length)(time) $^{-\alpha}$ whose value is determined by a procedure we discuss below.

With this similarity transformation, the equations of motion and heat conduction reduce to

$$U' - (1-U)(\ln G)' + (n-k_\rho)U = 0, \quad (73)$$

$$(1-U)U' + U(\alpha^{-1} - U) = \Theta [\ln(\xi^{2-k_\rho} G \Theta)]', \quad (74)$$

$$2[U' + nU - \mu(\alpha^{-1} - 1)] = \mu(1-U)[\ln(\xi^2 \Theta)]' + \beta_0 \Theta^b G^{a-1} \xi^{(2b-1)/\alpha} \left((\ln \Theta)'' + [\ln(\xi^2 \Theta)]' \right) \times \left\{ n-2+a[\ln(\xi^{-k_\rho} G)]' + (b+1)[\ln(\xi^2 \Theta)]' \right\}, \quad (75)$$

where $(\cdot)' \equiv d(\cdot)/d \ln \xi$, $\mu = 2/(\gamma-1)$, and

$$\beta_0 = \frac{2\chi_0(\alpha\zeta^{1/\alpha})^{2b-1}}{\Gamma^{b+1}g_0^{1-\alpha}} \text{sgn}(t). \quad (76)$$

This constitutes a fourth-order system of nonlinear ordinary differential equations. All physical solutions to these equations pass through two discontinuities, a heat front and a shock front, with the heat front at larger radius. However, the jump conditions for these discontinuities are easy to determine, and one can integrate between them. For a given β_0 , the solution depends only on the dimensionless parameter

$$\Omega = \frac{2\chi_0}{\Gamma^{b+1}g_0^{1-a}} \left(\frac{E_0}{g_0} \right)^{b-1/2}, \quad (77)$$

which measures the strength of the explosion. Large values of Ω constitute “strong” explosions, and the ratio of heat front radius to shock front radius is a monotonically increasing function of Ω . It is important at this point to add a cautionary note. In deriving the similarity solution, we assumed that radiation energy density is negligible in comparison to gas energy density. This cannot strictly be true at early times, since at $t=0$ the temperature diverges at the origin, and the radiation energy density

varies as T to a higher power than the gas energy density. However, the true behavior should approach the similarity solution at later times.

While we have reduced the gas dynamical equations to a system of ordinary differential equations that is trivial to integrate, solving the full problem is complex because the equations still depend on the unknown parameter β_0 , which in turn depends on ζ . To solve the problem, we must determine β_0 from the given initial conditions. Reinicke & Meyer-ter-Vehn (1991) describe the iteration procedure required to do this in detail, and we only summarize it here. To find a solution, one first chooses a value $\xi_h > 1$ for the dimensionless radius of the heat front, applies the boundary conditions at the front, and guesses a corresponding value of β_0 . For each ξ_h , there exists a unique β_0 for which it is possible to integrate the equations back from $\xi = \xi_h$ to the location of the shock front at $\xi = \xi_s$, apply the shock jump conditions, and continue integrating back to the origin at $\xi = 0$ without having the solution become double-valued and thus unphysical. One iterates to identify the allowed value of β_0 for the chosen ξ_h , and this gives the unique density, velocity, and temperature profiles allowed for that ξ_h . However, the solution one finds in this way may not correspond to the desired value of Ω . Reinicke & Meyer-ter-Vehn show that

$$\Omega = \beta_0 \left[2\pi \int_0^{\xi_h} \xi^{n-k_\rho+1} G(U^2 + \mu\Theta) d\xi \right]^{b-1/2}. \quad (78)$$

Thus, each choice of ξ_h corresponds to a particular value of Ω , and one must iterate a second time to find the value of ξ_h that gives the value of Ω determined from the input physical parameters of the problem. Alternately, instead of specifying a desired value of Ω , one can specify a ratio $R = \xi_h/\xi_s$, which also determines a unique value for ξ_h .

For our comparison between the semianalytic solution and Orion, we adopt the parameters $\gamma = 7/5$, $c_v = 1/(\gamma-1)$, $a = -2$, $b = 6$, $g_0 = \chi_0 = 1$, and $E_0 = 135$, which yields a strength $\Omega = 1.042 \times 10^{12}$ and a ratio $R = 2.16$. In the simulation, we turn off terms in the code involving radiation pressure and forces, and we set $\lambda = 1/3$ exactly. We use one-dimensional spherical polar coordinates rather than Cartesian coordinates; the solution procedures for this are identical to the ones outlined in § 4, with the exception that the gradient and divergence operators have their spherical rather than Cartesian forms, and the cell-centered finite differences are modified appropriately. Our computational domain covers $0 \leq r \leq 1.05$, is resolved by 256, 512, or 1024 cells, and has reflecting inner and outer boundary conditions. To initialize the problem we set initial density to the power-law profile $\rho = r^{-k_\rho}$ (with k_ρ set from eq. [67]), the initial velocity to zero, and the initial energy density to a small value, except in the cell adjacent to the origin, where its value is $\rho e = 135/(\gamma-1)$.

Figures 3, 4, and 5 compare the semianalytic density, velocity, and temperature profiles to the values we obtain from Orion after running to a time $t = 0.06$. As the plots show, the Orion results agree very well with the semianalytic solution, and the agreement improves with increasing resolution. In the lowest resolution run, there is a small oscillation in the density and velocity about a third of the way to the shock, which is likely due to the initial blast energy being deposited in a finite-volume region rather than as a true δ -function. However, this vanishes at higher resolutions. Overall, the largest errors are in the temperature in the shocked gas.

As a metric of convergence, we plot the error of our simulation relative to the analytic solution as a function of resolution in Figure 6. We do this for the quantities r_h and r_s , the positions

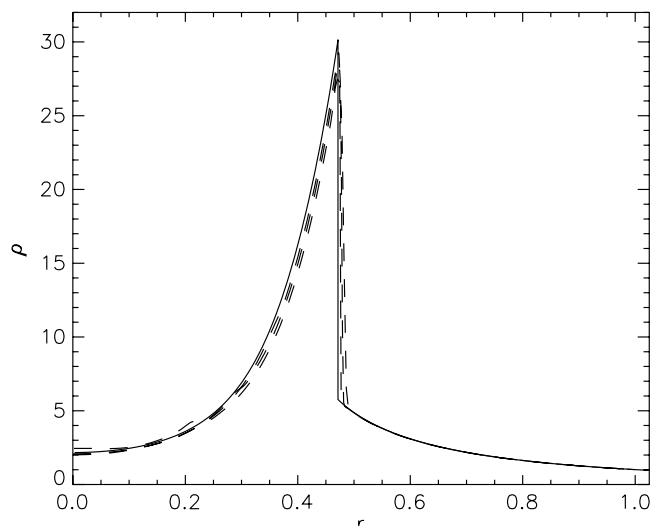


FIG. 3.—Density ρ vs. radius r for the radiating blast wave test. We show the semianalytic solution (solid line) and the Orion results at resolutions of 256, 512, and 1024 cells (dashed lines). The 256 cell run is the dashed line furthest from the semianalytic solution, and the 1024 cell run is the dashed line closest to it.

of the shock and heat fronts, and their ratio R . For this purpose, we define the location of the heat and shock fronts for the simulations as the positions of the cell edges where dT/dr and $d\rho/dr$ are most negative. As the plot shows, at the highest resolution the errors in all three quantities are $\lesssim 3\%$, and the calculation appears to be converging. The order of convergence is roughly 0.6 in all three quantities. It is worth noting that computing the locations of the heat and shock fronts is a particularly strong code test, because obtaining the correct propagation velocities for the two fronts requires that the code conserve total energy very well. Nonconservative codes have significant difficulties with this test (Timmes et al. 2006).

5.3. Radiation Pressure Tube

Our third test is to simulate a tube filled with radiation and gas. The gas within the tube is optically thick, so the diffusion approximation applies. The two ends of the tube are held at fixed radiation and gas temperature, and radiation diffuses through the

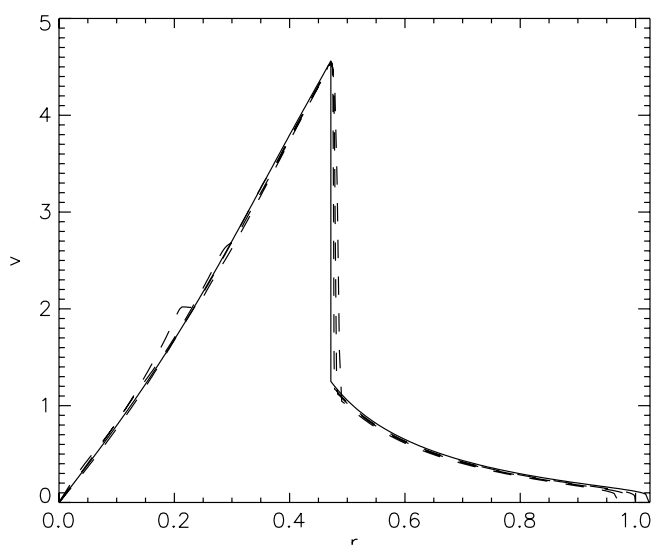


FIG. 4.—Same as Fig. 3, but for the velocity v .

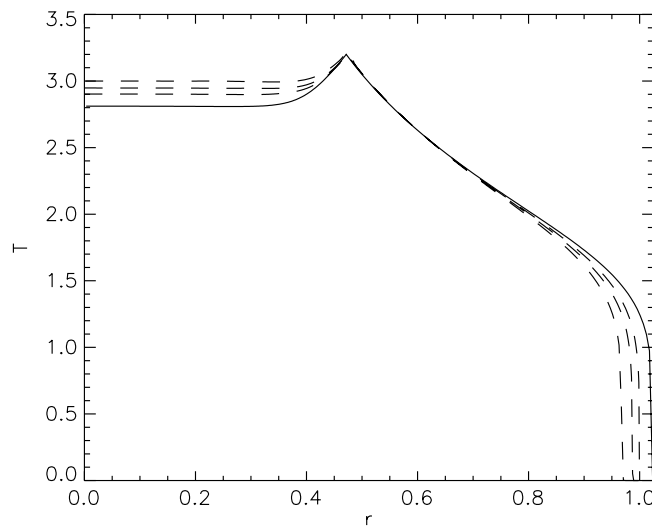


FIG. 5.—Same as Fig. 3, but for the temperature T .

gas from one end of the tube to the other. The radiation flowing through the tube exerts a force on the gas, and the gas density profile is such that, with radiation pressure, the gas is in pressure balance and should be stationary. For computational simplicity, we set the Rosseland and Planck mean opacities per unit mass of the gas to a constant value κ . A simulation of this system tests our code's ability to compute accurately the radiation pressure force in the very optically thick limit.

We first derive a semianalytic solution for the configuration of the tube satisfying our desired conditions. Since the gas is very optically thick and we are starting the system in equilibrium, we set $T_{\text{rad}} = T_{\text{gas}} \equiv T$. The fluid is initially at rest. The condition of pressure balance amounts to setting $\partial(\rho v)/\partial t + \nabla \cdot (\rho v v) = 0$ in equation (40), so that the radiation pressure force balances the gas pressure gradient. Thus, we have

$$\frac{dP}{dx} + \lambda \frac{dE}{dx} = 0, \quad (79)$$

$$\left(\frac{k_B}{\mu} \rho + \frac{4}{3} a_R T^3 \right) \frac{dT}{dx} + \frac{k_B}{\mu} T \frac{d\rho}{dx} = 0. \quad (80)$$

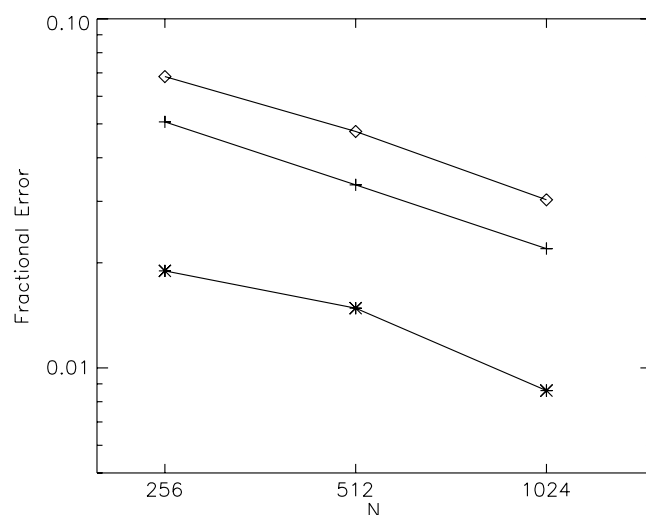


FIG. 6.—Fractional error vs. resolution N in the radiating blast wave test. The fractional error is defined as $|(\text{simulation value}) - (\text{analytic value})|/(\text{analytic value})$. We show error in the heat front radius r_h (plus signs), shock front radius r_s (asterisks), and their ratio $R = r_h/r_s$ (diamonds).

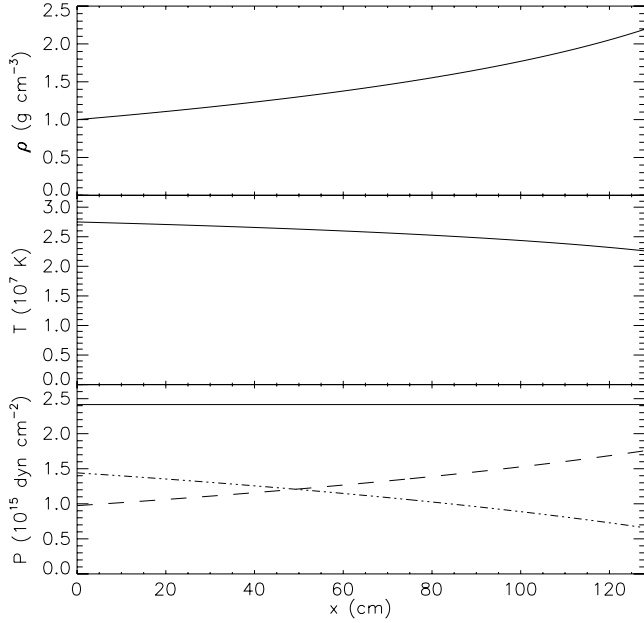


FIG. 7.—Density, temperature, and pressure vs. position in the radiation tube problem. The bottom panel shows total pressure (solid line), gas pressure (dashed line), and radiation pressure (double-dot-dashed line).

In the second step we have set $E = a_R T^4$ and $P = \rho k_B T / \mu$, where μ is the mean particle mass, and we have set $\lambda = 1/3$ as is appropriate for the optically thick limit. The radiation energy equation (48) for our configuration is simply

$$\frac{d}{dx} \left(\frac{c\lambda}{\kappa\rho} \frac{dE}{dx} \right) = 0, \quad (81)$$

$$\frac{d^2 T}{dx^2} + 3 \frac{1}{T} \left(\frac{dT}{dx} \right)^2 - \frac{1}{\rho} \left(\frac{d\rho}{dx} \right) \left(\frac{dT}{dx} \right) = 0. \quad (82)$$

Equations (80) and (82) are a pair of coupled nonlinear ordinary differential equations for T and ρ . The combined degree of the system is three, so we need three initial conditions to solve them. Thus, let the tube run from $x = x_0$ to x_1 , with temperature, density, and density gradient T_0 , ρ_0 , and $(d\rho/dx)_0$ at x_0 . For a given choice of initial conditions, it is trivial to solve equations (80) and (82) numerically to find the density and temperature profile. We wish to investigate both the radiation pressure- and gas pressure-dominated regimes, so we choose parameters to ensure that our problem covers both. The choice $x_0 = 0$, $x_1 = 128$ cm, $\rho_0 = 1$ g cm $^{-3}$, $(d\rho/dx)_0 = 5 \times 10^{-3}$ g cm $^{-4}$, and $T_0 = 2.75 \times 10^7$ K satisfies this requirement if we adopt $\mu = 2.33m_p = 3.9 \times 10^{-24}$ g, and $\kappa = 100$ cm 2 g $^{-1}$. Figure 7 shows the density, temperature, and pressure as a function of position for these parameters.

We solve the equations to obtain the density and temperature as a function of position and then set these values as initial conditions in a simulation. The simulation has 128 cells along the length of the tube on the coarsest level. We impose Dirichlet boundary conditions on the radiation field, with the radiation temperature at each end of the tube set equal to its value as determined from the analytic solution. We use symmetry boundary conditions on the hydrodynamics, so that gas can neither enter nor leave the computational domain. To ensure that our algorithm does not encounter problems at the boundaries between AMR levels, we refine the central 1/4 of the problem domain to double the resolution of the base grid. We evolve the

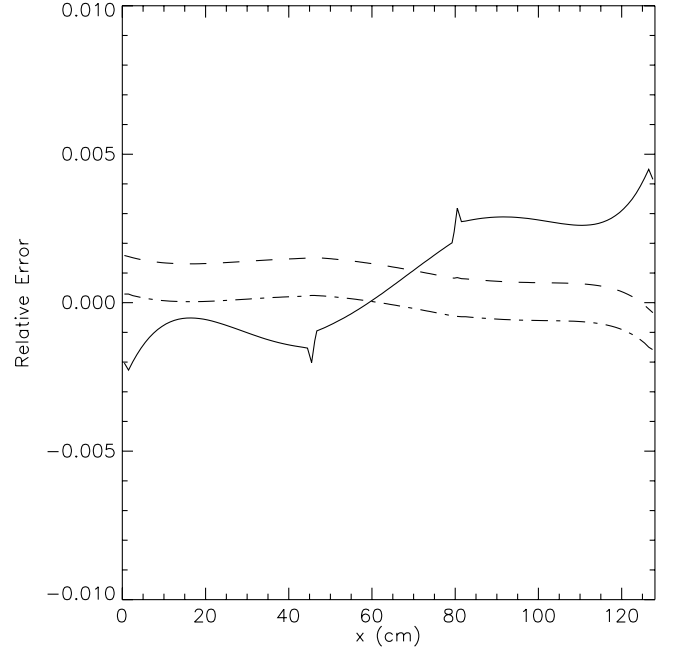


FIG. 8.—Relative error in density (solid line), gas temperature (dashed line), and radiation temperature (dot-dashed line) in the radiation tube test.

system for 10 sound crossing times and measure the amount by which the density and temperature change relative to the exact solution. We plot the relative error, defined as $[(\text{numerical solution}) - (\text{analytic solution})] / (\text{analytic solution})$, in the density, gas temperature, and radiation temperature in Figure 8. As the plot shows, our numerical solution agrees with the analytic result to better than 0.5% throughout the computational domain. The density error is smallest in the higher resolution central region, as expected. There is a very small increase in error at level boundaries, but it is still at the less than 0.5% level.

5.4. Radiation-inhibited Bondi Accretion

The previous test focuses on radiation pressure forces in the optically thick limit. To test the optically thin limit, we simulate accretion onto a radiating point particle. We consider a point mass M radiating with a constant luminosity L accreting from a background medium. The medium consists of gas which has zero velocity and density ρ_∞ far from the particle. We take the gas to be isothermal with constant temperature T and enforce that it is not heated or cooled radiatively by setting its Planck opacity $\kappa_{0P} = 0$. We set the Rosseland opacity of the gas to a constant nonzero value κ_{0R} and choose ρ_∞ such that the computational domain is optically thin. In this case, the radiation free-streams away from the point mass, and the radiation energy density and radiative force per unit mass on the gas are

$$E = \frac{L}{4\pi r^2 c}, \quad (83)$$

$$\mathbf{f}_{\text{rad}} = \frac{\kappa_{0R} L}{4\pi r^2 c} \left(\frac{\mathbf{r}}{r} \right), \quad (84)$$

where \mathbf{r} is the radial vector from the particle and r is its magnitude. The gravitational force per unit mass is $\mathbf{f}_{\text{grav}} = -(GM/r^2)(\mathbf{r}/r)$, so the net force per unit mass is

$$\mathbf{f} = \mathbf{f}_{\text{rad}} + \mathbf{f}_{\text{grav}} = -(1 - f_{\text{Edd}}) \frac{GM}{r^2} \left(\frac{\mathbf{r}}{r} \right), \quad (85)$$

where

$$f_{\text{Edd}} = \frac{\kappa_{0R} L}{4\pi G M c} \quad (86)$$

is the fraction of the Eddington luminosity with which the point mass is radiating.

Since the addition of radiation does not alter the $1/r^2$ dependence of the specific force, the solution is simply the standard Bondi (1952) solution but for an effective mass of $(1 - f_{\text{Edd}})M$. The accretion rate is the Bondi rate

$$\dot{M}_B = 4\pi \xi r_B^2 c_s \rho_\infty, \quad (87)$$

where

$$r_B = (1 - f_{\text{Edd}}) \frac{GM}{c_s^2} \quad (88)$$

is the Bondi radius for the effective mass, c_s is the gas sound speed at infinity, and ξ is a numerical factor of order unity that depends on the gas equation of state. For an isothermal gas, $\xi = e^{3/2}/4$ and the radial profiles of the nondimensional density $\alpha \equiv \rho/\rho_\infty$ and velocity $u \equiv v/c_s$ are given by the solutions to the nonlinear algebraic equations (Shu 1992)

$$x^2 \alpha u = \xi, \quad (89)$$

$$\frac{u^2}{2} + \ln \alpha - \frac{1}{x} = 0, \quad (90)$$

where $x \equiv r/r_B$ is the dimensionless radius.

To set up this test, we make use of the Lagrangian sink particle algorithm of Krumholz et al. (2004) coupled with the “star particle” algorithm of Krumholz et al. (2007) which allows the sink particle to act as a source of radiation. We refer readers to those papers for details on the sink and star particle algorithms. We simulate a computational domain 5×10^{13} cm on a side, resolved by 256^3 cells, with a particle of mass $M = 10 M_\odot$ and luminosity $L = 1.6 \times 10^5 L_\odot$ at its center. We adopt fluid properties $\rho_\infty = 10^{-18} \text{ g cm}^{-3}$, $\kappa_{0R} = 0.4 \text{ cm}^2 \text{ g}^{-1}$, and $c_s = 1.3 \times 10^7 \text{ cm s}^{-1}$, corresponding to a gas of pure, ionized hydrogen with a temperature of 10^6 K. With these values, $f_{\text{Edd}} = 0.5$, $r_B = 4.0 \times 10^{12}$ cm, and $\dot{M}_B = 2.9 \times 10^{17} \text{ g s}^{-1}$. We use inflow boundary conditions on the gas and Dirichlet boundary conditions on the radiation field, with the radiation energy density on the boundary set to the value given by equation (83).

Figure 9 compares the steady state density α and velocity u computed by Orion to the analytic solution. The agreement is excellent, with differences between the analytic and numerical solutions of $\sim 1\%$ everywhere except very near the accretion radius at $x = 0.25$. The maximum error is $\sim 10\%$ at the surface of the accretion region; this is comparable to the error in density for nonradiative Bondi accretion with similar resolution in Krumholz et al. (2004). In comparison, the solution is nowhere near the solution that would be obtained without radiation. After running for five Bondi times ($= r_B/c_s$), the average accretion rate is $2.4 \times 10^{17} \text{ g s}^{-1}$. While this differs from the analytic solution by 19%, the error is also not tremendously different from that obtained by Krumholz et al. (2004), when the Bondi radius was resolved by four accretion radii, and is nowhere near the value of $1.2 \times 10^{18} \text{ g s}^{-1}$ which would occur without radiation.

We should at this point mention one limitation of our algorithm, as applied on an adaptive grid, that this test reveals. The

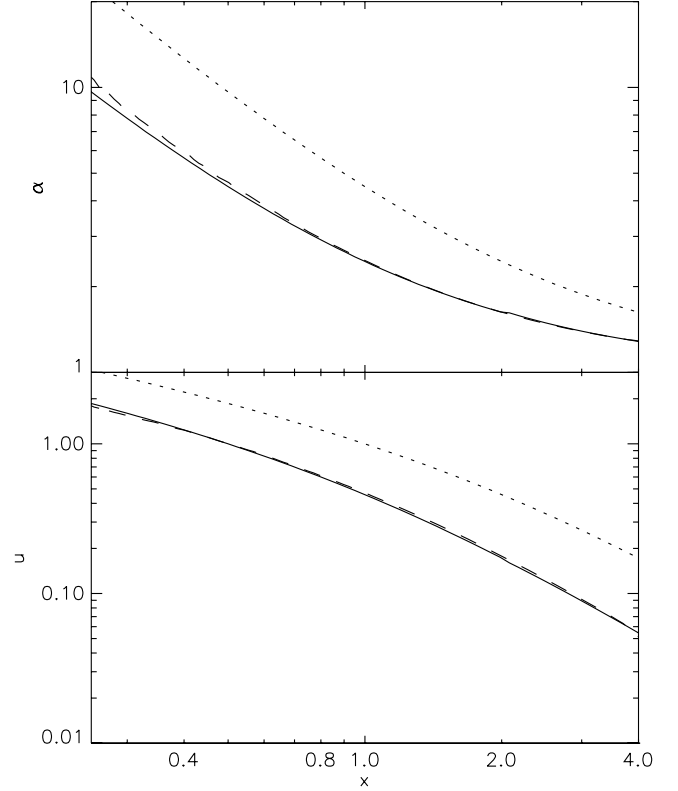


FIG. 9.—Dimensionless density α (top) and velocity u (bottom) vs. dimensionless position x for radiation-inhibited Bondi accretion. We show the analytic solution (solid lines), the solution as computed with Orion (dashed lines), and the analytic solution for Bondi accretion without radiation (dotted lines). For the Orion result, the values shown are the radial averages computed in 128 logarithmically spaced bins running from the accretion radius $x = 0.25$ to the outer edge of the computational domain $x = 5$.

$1/r^2$ gradient in the radiation energy density is very steep, and we compute the radiation force by computing gradients in E . We found that, in an AMR calculation, differencing this steep gradient across level boundaries introduced significant artifacts in the radiation pressure force. With such a steep gradient, we were only able to compute the radiation pressure force accurately on fixed grids, not adaptive grids. This is not a significant limitation for most applications, however, since for any appreciable optical depth the gradient will be much shallower than $1/r^2$. As the radiation pressure tube test in § 5.3 demonstrates, in an optically thick problem the errors that arise from differencing across level boundaries are less than 1%.

5.5. Advecting Radiation Pulse

The previous two tests check our ability to compute the radiation pressure force accurately in the optically thick and optically thin limits. However, they do not strongly test radiation advection by gas. To check this, we simulate a diffusing, advecting radiation pulse. The initial condition is a uniform background of gas and radiation far from the pulse. Centered on $x = 0$, there is an increase in the radiation energy density and a corresponding decrease in the gas density, so that the initial condition is everywhere in pressure balance. As radiation diffuses out of the pulse, pressure support is lost and the gas moves into the lower density region. We cannot solve this problem analytically, but we can still perform a very useful test of the methodology by comparing a case in which the gas is initially at rest with respect to the computational grid with a case in which the gas is moving at a

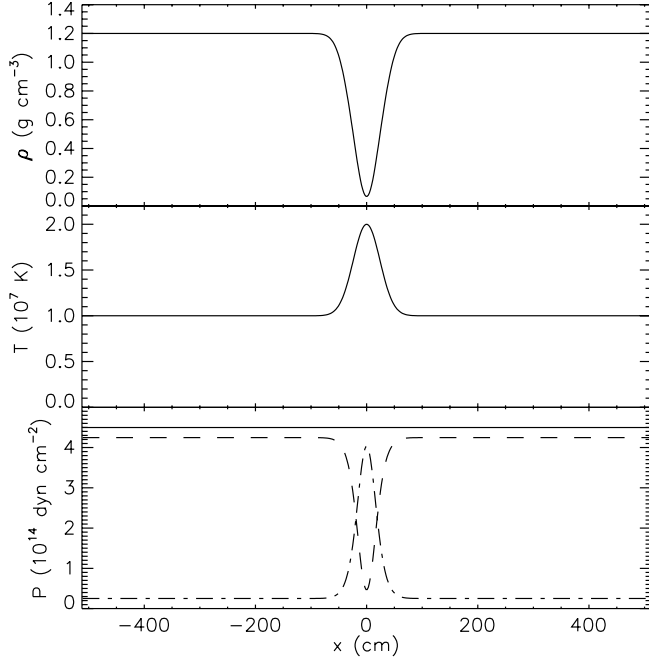


FIG. 10.—Density, temperature, and pressure vs. position in the advected radiation pulse problem. The bottom panel shows total pressure (*solid line*), gas pressure (*dashed line*), and radiation pressure (*dot-dashed line*).

constant velocity with respect to the grid. The results should be identical when shifted to lie on top of one another, but the work and advection terms will be different in the stationary case from those in the advected case. Checking that the results do not change when we advect the problem enables us to determine if our code is correctly handling the advection of radiation by the gas.

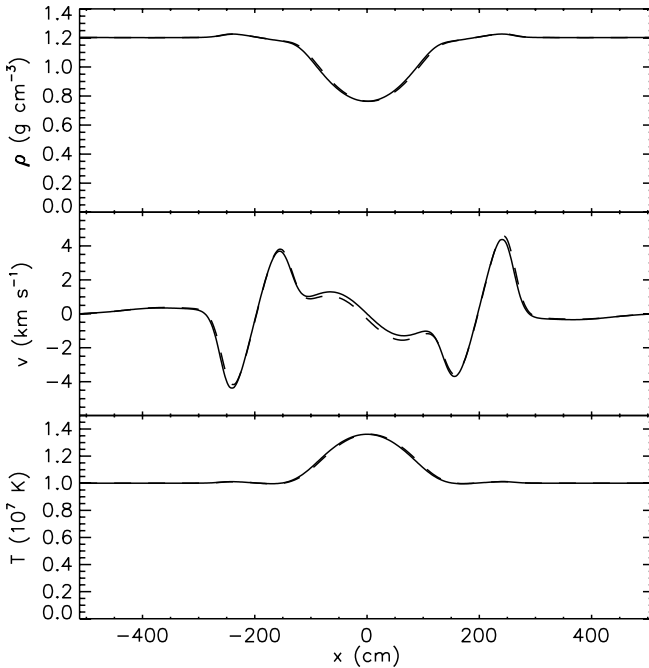


FIG. 11.—Density, velocity, and temperature in the advected radiation pulse problem after 4.8×10^{-5} s of evolution. In each panel the solid line is the unadvected run, and the dashed line is the advected run shifted 48 cm in the $-x$ -direction. In the velocity plot, the velocity we show for the advected run is relative to the overall systematic velocity of 10^6 cm s $^{-1}$ in the initial condition.

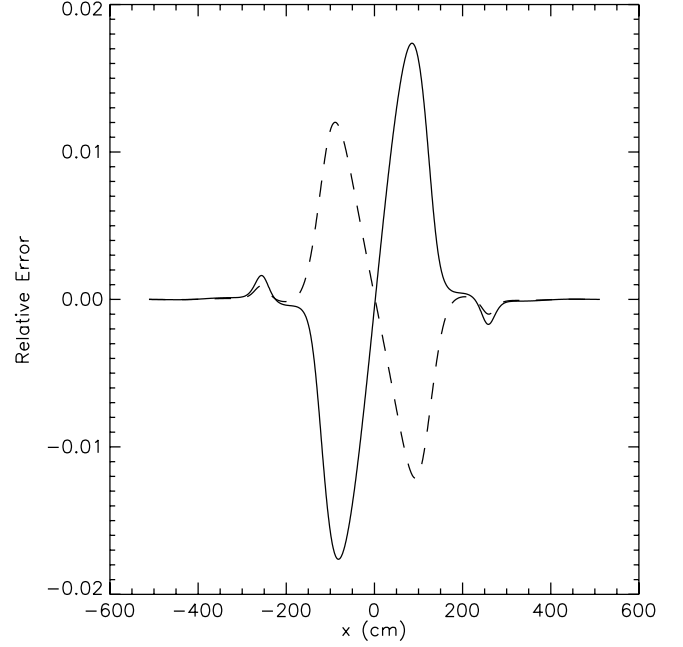


FIG. 12.—Relative error in density (*solid line*) and gas/radiation temperature (*dashed line*) in the radiation pulse test.

For our simulations, we use equal initial gas and radiation temperatures, with temperature and density profiles

$$T = T_0 + (T_1 - T_0) \exp\left(-\frac{x^2}{2w^2}\right), \quad (91)$$

$$\rho = \rho_0 \frac{T_0}{T} + \frac{a_R \mu}{3k_B} \left(\frac{T_0^4}{T} - T^3 \right), \quad (92)$$

with $T_0 = 10^7$ K, $T_1 = 2 \times 10^7$ K, $\rho_0 = 1.2$ g cm $^{-3}$, $w = 24$ cm, $\mu = 2.33m_p = 3.9 \times 10^{-24}$ g, and $\kappa = 100$ cm 2 g $^{-1}$. The density, temperature, and pressure profiles are shown in Figure 10. In the bottom panel, the solid line is the total pressure, the dashed line is the gas pressure, and the dot-dashed line is the radiation pressure. As the figure indicates, the system is initially in pressure balance.

We compare two runs, one where the velocity is zero everywhere and another with a uniform initial velocity $v = 10^6$ cm s $^{-1}$ in the x -direction. In both runs the simulation domain extends from -512 to 512 cm, resolved by 512 cells with no adaptivity. We use periodic boundary conditions on the gas and the radiation and run for 4.8×10^{-5} s, long enough for the pulse to have been advected over its own initial width twice.

To check our results, we shift the advected run by 48 cm in the $-x$ -direction, so that it should lie on top of the unadvected run. Figure 11 shows the configuration of the advected and unadvected runs at this point. We then plot the relative difference between the advected and unadvected runs, defined as (unadvected $-$ advected)/unadvected, in Figure 12. We do not differentiate between the gas and radiation temperatures, because they are identical at the 10^{-3} level. We do not plot the error in velocity because the velocities in the unadvected run are close to zero over most of the computational domain. As the plot shows, the difference between the advected and unadvected runs is less than 2% everywhere in the simulation.

6. SUMMARY

We derive the correct equations for mixed-frame flux-limited diffusion radiation hydrodynamics. The error in our equations if

of order v^2/c^2 in the static diffusion limit and of order v/c in the dynamic diffusion and streaming limits. We give the equations in a form that is well suited to implementation in numerical simulations, because they make it trivial to maintain exact conservation of total energy. Our analysis reveals that lower order formulations of the equations, which neglect differences between the laboratory and comoving frames, are incorrect at order unity for systems in the dynamic diffusion limit. It remains to be seen how serious this defect is in practice, but analytic arguments suggest that at a minimum one ought to be very careful in applying zeroth-order codes to problems where there are interesting or important structures on scales for which $\beta\tau \sim 1$. We give the equations that are correct to leading order for dynamic diffusion, which do not suffer from this problem.

Our analysis also reveals that, for static diffusion problems, one can obtain a significant algorithmic simplification and speedup compared to algorithms based on comoving-frame formulations of the equations by treating nondominant radiation terms explicitly rather than implicitly. This advance is possible even though the underlying equations of our method conserve total energy to machine precision while comoving-frame formulations of the equations do not. This property is particularly important for flows that are turbulent or otherwise involve large gradients in gas or radiation properties, since these are the problems most likely to suffer from numerical nonconservation. We demonstrate an implementation of this method in the Orion adaptive mesh refinement code and show that it provides excellent agree-

ment with analytic and semianalytic solutions in a series of test problems covering a wide range of radiation hydrodynamic regimes.

We thank J. I. Castor and J. M. Stone for helpful comments on the manuscript and T. A. Thompson for helpful discussions. We also thank the referee for comments that improved the paper. Support for this work was provided by NASA through Hubble Fellowship grant HSF-HF-01186 awarded by the Space Telescope Science Institute, which is operated by the Association of Universities for Research in Astronomy, Inc., for NASA, under contract NAS 05-26555 (M. R. K.); NASA ATP grants NAG 05-12042 and NNG 06-GH96G (R. I. K. and C. F. M.); the US Department of Energy at the Lawrence Livermore National Laboratory under contract W-7405-Eng-48 (R. I. K. and J. B.); and the NSF through grants AST 00-98365 and AST 06-06831 (C. F. M.). This research was also supported by grants of high-performance computing resources from the Arctic Region Supercomputing Center; the NSF San Diego Supercomputer Center through NPACI program grant UCB267; the National Energy Research Scientific Computing Center, which is supported by the Office of Science of the US Department of Energy under contract DE-AC03-76SF00098, through ERCAP grant 80325; and the US Department of Energy at the Lawrence Livermore National Laboratory under contract W-7405-Eng-48.

APPENDIX

SCALINGS IN THE DYNAMIC DIFFUSION LIMIT

Here we show that the emission minus absorption term $4\pi B/c - E$ is of order $\beta^2 E$ in the dynamic diffusion limit. Mihalas & Weibel-Mihalas (1999) argue that in this limit $4\pi B/c - E$ is of order $(\beta/\tau)E$. However, this conclusion is based on their analysis of the second-order equilibrium diffusion approximation (Mihalas & Weibel-Mihalas 1999, p. 461–466), in which they retain terms of order β/τ while dropping those of order β^2 . While this is correct for static diffusion, in the dynamic diffusion limit $\beta^2 \gg \beta/\tau$, so the approach in Mihalas & Weibel-Mihalas is not consistent and is insensitive to terms of order β^2 .

We do not give a general proof that $4\pi B/c - E \sim \beta^2 E$ for dynamic diffusion, but we can establish it by a simple thought experiment. Consider a system that is infinitely far into the dynamic diffusion limit, in the sense that $\tau = \infty$: an infinite uniform medium that is at rest and in perfect thermal equilibrium between the radiation field and the gas. In the rest frame of the medium, these assumptions require $E_0 = 4\pi B/c$, $\mathbf{F}_0 = 0$, and $\mathbf{P}_0 = (E_0/3)\mathbf{I}$. Now consider an observer moving at velocity \mathbf{v} relative to the medium. In the observer's frame, $4\pi B/c$ is the same because the gas temperature T_0 is a world-scalar, and the Lorentz transform to all orders for the energy gives

$$E = \gamma^2 \left[E_0 + 2 \frac{\mathbf{v} \cdot \mathbf{F}_0}{c^2} + \frac{(\mathbf{v} \mathbf{v})}{c^2} : \mathbf{P}_0 \right] \quad (\text{A1})$$

$$= \gamma^2 \left[1 + \frac{1}{3} \left(\frac{v^2}{c^2} \right) \right] \left(\frac{4\pi B}{c} \right) \quad (\text{A2})$$

$$= \left(\frac{4\pi B}{c} \right) \left[1 + \frac{4}{3} \left(\frac{v^2}{c^2} \right) + O\left(\frac{v^4}{c^4} \right) \right]. \quad (\text{A3})$$

Thus, for this case it is clear that $4\pi B/c - E \sim \beta^2 E$ to leading order.

Note that using the correct scaling is necessary to obtain sensible behavior from the equations in the dynamic diffusion limit. If one assumes that $4\pi B/c - E \sim (\beta/\tau)E$, then in the gas and radiation energy equations (41) and (42) in the dynamic diffusion limit, the term $\kappa_{0P}(v^2/c)[(3 - R_2)/2]E$ is of higher order than any other term except perhaps the time derivative. Since this term is nonzero for any system with nonzero velocity, opacity, and radiation energy density, this means that there would be no way for the time derivative term to ever vanish. Thus, a system in the dynamic diffusion limit could never be in equilibrium unless its velocity or radiation energy were zero everywhere. Clearly, this cannot be correct, since it predicts that our static, infinite, uniform medium cannot be in equilibrium when seen by an observer moving by at velocity \mathbf{v} , even though it is manifestly in equilibrium in its own rest frame. On the other hand, if we take $4\pi B/c - E = (4/3)(v^2/c^2)E$, as computed from the Lorentz transform, it is trivial to verify that equations (41) and (42) correctly give $\partial(\rho e)/\partial t = \partial E/\partial t = 0$, and $(G^0, \mathbf{G}) = (0, 0)$ as well. The observer sees a flux that does work on the gas, but this is precisely canceled by a mismatch between emission and absorption of radiation by the gas, leading to zero net energy transfer.

REFERENCES

- Alme, M. L., & Wilson, J. R. 1973, *ApJ*, 186, 1015
- Bondi, H. 1952, *MNRAS*, 112, 195
- Castor, J. I. 1972, *ApJ*, 178, 779
- . 2004, *Radiation Hydrodynamics* (Cambridge: Cambridge Univ. Press)
- Crockett, R. K., Colella, P., Fisher, R. T., Klein, R. I., & McKee, C. F. 2005, *J. Comput. Phys.*, 203, 422
- Fisher, R. T. 2002, Ph.D. thesis, Univ. California, Berkeley
- Hayes, J. C., Norman, M. L., Fiedler, R. A., Bordner, J. O., Li, P. S., Clark, S. E., ud-Doula, A., & Mac Low, M.-M. 2006, *ApJS*, 165, 188
- Howell, L. H., & Greenough, J. A. 2003, *J. Comput. Phys.*, 184, 53
- Hubeny, I., & Burrows, A. 2007, *ApJ*, 659, 1458
- Kippenhahn, R., & Weigert, A. 1994, *Stellar Structure and Evolution* (Berlin: Springer)
- Klein, R. I. 1999, *J. Comp. Appl. Math.*, 109, 123
- Krumholz, M. R., Klein, R. I., & McKee, C. F. 2007, *ApJ*, 656, 959
- Krumholz, M. R., McKee, C. F., & Klein, R. I. 2004, *ApJ*, 611, 399
- . 2005, *ApJ*, 618, L33
- Levermore, C. D. 1984, *J. Quant. Spectrosc. Radiat. Transfer*, 31, 149
- Levermore, C. D., & Pomraning, G. C. 1981, *ApJ*, 248, 321
- Lowrie, R. B., & Morel, J. E. 2001, *J. Quant. Spectrosc. Radiat. Transfer*, 69, 475
- Lowrie, R. B., Morel, J. E., & Hittinger, J. A. 1999, *ApJ*, 521, 432
- Mihalas, D., & Auer, L. H. 2001, *J. Quant. Spectrosc. Radiat. Transfer*, 71, 61
- Mihalas, D., & Klein, R. I. 1982, *J. Comput. Phys.*, 46, 97
- Mihalas, D., & Weibel-Mihalas, B. 1999, *Foundations of Radiation Hydrodynamics* (New York: Dover)
- Miniati, F., & Colella, P. 2007, *J. Comput. Phys.*, 224, 519
- Pember, R. B. 1993, *SIAM J. Sci. Computing*, 14, 824
- Pomraning, G. C. 1983, *ApJ*, 266, 841
- Puckett, E. G., & Saltzman, J. S. 1992, *Physica D*, 60, 84
- Reinicke, P., & Meyer-ter-Vehn, J. 1991, *Phys. Fluids*, 3, 1807
- Shestakov, A. I. 1999, *Phys. Fluids*, 11, 1091
- Shestakov, A. I., & Greenough, J. A. 2001, *AMRH and the High Energy Reinicke Problem*, Tech. Rep. UCRL-ID-143937 (Livermore: LANL)
- Shu, F. H. 1992, *Physics of Astrophysics*, Vol. II (Mill Valley: University Science)
- Su, B., & Olson, G. L. 1996, *J. Quant. Spectrosc. Radiat. Transfer*, 56, 337
- Thompson, T. A., Quataert, E., & Murray, N. 2005, *ApJ*, 630, 167
- Timmes, F. X., Fryxell, B., & Hrbek, G. M. 2006, *Spatial-Temporal Convergence Properties of the Tri-Lab Verification Test Suite in 1D for Code Project A*, Tech. Rep. LA-UR-06-6444 (Los Alamos: LANL)
- Truelove, J. K., Klein, R. I., McKee, C. F., Holliman, J. H., Howell, L. H., Greenough, J. A., & Woods, D. T. 1998, *ApJ*, 495, 821
- Turner, N. J., & Stone, J. M. 2001, *ApJS*, 135, 95
- Turner, N. J., Stone, J. M., Krolik, J. H., & Sano, T. 2003, *ApJ*, 593, 992
- Whitehouse, S. C., & Bate, M. R. 2004, *MNRAS*, 353, 1078
- Whitehouse, S. C., Bate, M. R., & Monaghan, J. J. 2005, *MNRAS*, 364, 1367